J. Fluid Mech. (1990), *vol.* 217, *pp.* 263–298
Printed in Great Britain

A spherical particle straddling a fluid/gas interface in an axisymmetric straining flow

By J. A. STOOS† AND L. G. LEAL‡
Department of Chemical Engineering, California Institute of Technology, Pasadena, California 91125, USA

(Received 4 May 1989 and in revised form 9 January 1990)

Numerical solutions, obtained via the boundary-integral technique, are used to consider the effect of a linear axisymmetric straining flow on the existence of steady-state configurations in which a neutrally buoyant spherical particle straddles a gas–liquid interface. The problem is directly applicable to predictions of the stability of particle capture in flotation processes, and is also of interest in the context of contact angle and surface tension measurements. A primary goal of the present study is a determination of the critical capillary number, Ca_c, beyond which an initially captured particle is pulled from the interface by the flow, and the dependence of Ca_c on the equilibrium contact angle θ_c. We also present equilibrium configurations for a wide range of contact angles and subcritical capillary numbers.

1. Introduction

The existence and form of solutions for the shape of a fluid interface contacting a solid boundary is important in a number of applications in fluid mechanics. For example, several methods of characterizing fluid/fluid interfacial tensions rely on the measurement of interface shapes or on the determination of the maximum external force at which an equilibrium interface shape exists in contact with a solid boundary (such as rings, plates, and spheres). (Princen 1963; Princen & Mason 1965*a*, *b*; Huh & Scriven 1969; Huh & Mason 1974; Boucher & Evans 1975; Boucher, Evans & Kent 1976; Boucher & Kent 1977; Hiemenz 1977; Girault, Schiffrin & Smith 1982, 1984; Rotenberg, Boruvka & Neumann 1984, Smith & van de Ven 1984). Measurement of interfacial shapes is also an important tool in the determination of macroscopic contact angles, Rotenberg, Boruvka & Neumann (1983).

The study presented in this paper is motivated by the problem of capture stability for small particles at the surface of a bubble or drop in effluent and mineral flotation. The key question is whether the hydrodynamic and body forces which act on the particle once it has been swept to the rear of the bubble or drop will overcome capillary forces and pull the particle off the bubble. A first step toward answering this question is to determine conditions when an equilibrium configuration exists for the particle in the interface where all of the forces balance. Several researchers (Princen & Mason 1965; Huh & Scriven 1969; Huh & Mason 1974; Rapacchietta, Neumann & Omenyi 1977; Rappachietta & Neumann 1977; Boucher & Kent 1978; Boucher & Jones 1981) have, in fact, already investigated this question in the approximate case of a sphere or spheroid in a static fluid contacting an unbounded fluid/fluid interface.

† Current address: Mobil R. & D., Paulsboro, New Jersey 08066, USA.
‡ Current address: Department of Chemical and Nuclear Engineering, University of California at Santa Barbara, Santa Barbara, CA 93106, USA.

Because of the nonlinear nature of the Young–Laplace equation governing interfacial statics, solutions were obtained either as asymptotic approximations for nearly flat interfaces or by numerical techniques employing iterative methods to ensure that the boundary conditions and force balance on the particle were satisfied. The force balance on the particle, in this case, is between capillary forces which tend to maintain the particle on the interface, and body forces which usually tend to pull it off. Such analyses offer one way, in principle, of explaining the selective separations achieved by flotation based both on the size and chemical nature (i.e. contact angle) of the particle (Sutherland & Wark 1955; Derjaguin & Dukhin 1981). For example, one may be able to show that equilibrium configurations are possible for one component of a physical system but not for another component and to use this as a basis for evaluating the feasibility of selective separation of these components by flotation.

However, if such analyses are to accurately model the flotation problem, hydrodynamic effects must also be included. Hydrodynamic viscous forces may be of the same order of magnitude or larger than forces arising from density differences between the particles and fluids since the particles being removed are often nearly neutrally buoyant (which is one reason why effluent flotation is used). Thus, in situations with small interfacial tension forces (i.e. for small contact angles and/or small contact line lengths) the existence or absence of an equilibrium configuration may depend critically on the presence or absence of small viscous forces which tend to pull the particle from the interface. Thus hydrodynamic effects can promote selective separation and affect the separation efficiency in a manner that complements the effects of a density difference between the particle and the fluids.

In comparison to the many studies on the effect of density differences in the statics problem, the effect of viscous flow on the existence and form of solutions for flotation contact problems has received much less attention. Ranger (1978) and Falade (1982) investigated the motion of a disk straddling a flat interface in a creeping flow. Later, Davis (1982) considered a sphere contacting an unbounded interface in an extensional flow, but the interface was only allowed to undergo small deformations and solutions were obtained only for gravity and surface-tension-dominated cases for small differences in fluid viscosities. Unfortunately, none of these analyses is suitable for application to the flotation problem because of the limitations required on the magnitude of the viscous forces, the limited extent of the interface deformation and the small range of permissible contact angles ($\approx \frac{1}{2}\pi$). The only analysis that is focused directly upon the role of viscous forces on the stability of captured particles is due to French & Wilson (1980), who attempted to examine the effects of viscous forces on a cap of particles on a bubble. However, their main conclusion is that the action of the flow stabilizes the particles, rather than tending to pull them from the bubble surface, and this clearly contradicts physical intuition. It also disagrees with observations made in our laboratory (Stoos 1987) on the stability of a cap of particles on a bubble, where the bubble is held fixed on the tip of a syringe needle in flow through a capillary tube. The relative scarcity of theoretical investigations that include viscous effects is undoubtedly due to the complicated nature of the nonlinear free-boundary problem which must be solved. However, the solution of free-boundary problems at low Reynolds number via boundary-integral method has now become routine (cf. Youngren & Acrivos 1975, 1976; Rallison & Acrivos 1978; Lee & Leal 1982 and Stone, Bentley & Leal 1986). In the present paper, we use the boundary-integral technique to consider the prototype problem of a single spherical

particle contacting a free deformable interface in the presence of a steady, uniaxial extensional flow.

For this initial investigation we consider only the conditions for existence of steady-state configurations. In particular, we do not attempt to analyse the dynamics of particle removal when a steady state is not possible, nor do we concern ourselves with the transient regime prior to achieving a steady state. Thus, in spite of the fact that the related phenomena of contact line slip and dynamic contact angles could be included in the boundary-integral analysis by using one of the models available in the literature, cf. Dussan V. (1979), these effects are not included in the present work. Also line tension effects (Ivanov, Kralchevsky & Nikolov 1985; Kralchevsky, Ivanov & Nikolov 1985; Kralchevsky, Nikolov & Ivanov 1985; Nikolov, Kralchevsky & Ivanov 1985), which may be important for the very small particles found in flotation applications, have not been included explicitly in this study since we are assuming a macroscopic contact angle and macroscopic surface tension that have been correctly measured or calculated, taking into account the possible presence of these effects. Of course, line tension or film tension effects would have to be included explicitly in an additional force balance at the contact line if the solid particle were replaced by a small drop or bubble. Finally, surfactant effects and associated complications due to interface blockage, interfacial viscosity and spatial variations in surface tension have not been included in this initial investigation. It may be noted that Sadhal & Johnson (1983*a*, *b*) have considered the complementary problem of equilibrium configurations of a liquid layer on a solid particle.

2. Problem statement

The same 'flotation' approximations, based on the existence of two very different lengthscales, which have been used in the statics problem are also introduced in the flow problem that is analysed here. In particular, we assume that the radius of the particle a is very much smaller than the radius of the bubble R, so the the curvature of the bubble and any deformations of the bubble on the lengthscale R are not 'seen' by the particle, and the bubble surface appears flat to a leading order of approximation. Of course, deformations of the interface on a lengthscale a do influence the particle, and these must be considered explicitly to determine conditions for capture stability.

Upon contact, the particle is swept to the rear stagnation point of the bubble, where it is exposed to an axisymmetric flow that tends to pull it from the interface. By means of a 'local' approximation of the undisturbed flow, Stoos (1987) showed that, to leading order in (a/R), this flow is a linear uniaxial extensional flow. Approximating the full undisturbed flow as a linear uniaxial extensional flow centred at the rear stagnation point amounts to solving the first inner problem of a matched asymptotic analysis. Since the disturbance flow in the first inner problem will decay like $1/r$, it will give rise to additional flows in the outer region at $O(a/R)^2$, which, along with the deformation of the boundary shape resulting from the first inner problem, will modify the outer problem. However, even the leading-order inner problem is very difficult, requiring numerical solutions for the interface shape and the flow field, and it is not practical to attempt to evaluate higher-order terms in the expansion. From a pragmatic point of view, it is likely in any case that capture stability will be dominated by the lowest-order (a/R) extensional flow contribution, rather than by the $O(a/R)^2$ terms.

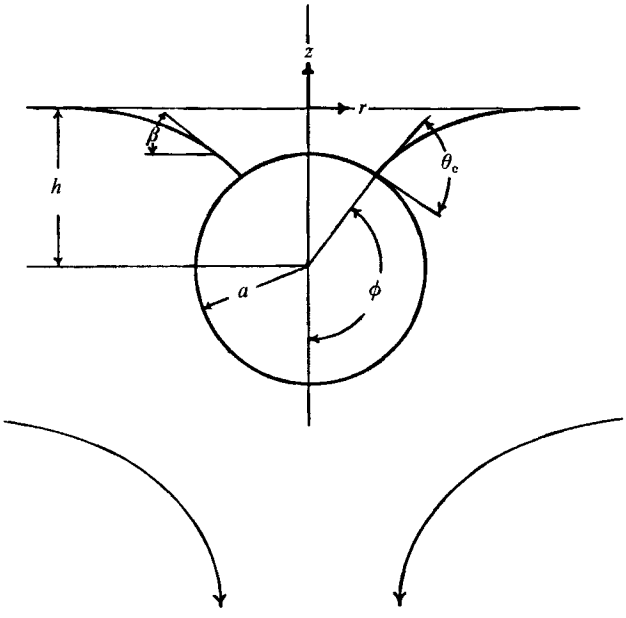

FIGURE 1. Schematic of problem.

Thus, as shown in figure 1, we consider the problem of a spherical particle of density ρ_p and radius a straddling a free interface between a liquid and a gas where the equilibrium contact angle is θ_c, the surface tension is a constant σ, and the density and viscosity of the incompressible Newtonian lower fluid are ρ and μ, respectively. The gas above the interface is assumed to have a negligible viscosity and density. In the axisymmetric problem the interface is represented in terms of cylindrical coordinates (r, z) centred on the plane of the undeformed interface with the sphere centre at $(O, -h)$. The position of the contact line on the sphere is designated by the angle ϕ, measured from the symmetry axis. The convention, shown in figure 1, of measuring ϕ from the *negative* z-axis has been used to maintain consistency with the nomenclature from earlier investigations of the statics problem. Also, as explained above, the interface is assumed to be flat, far from the particle, and the lower fluid approaches a uniaxial extensional flow $\boldsymbol{u}_\infty = G(-r\boldsymbol{i}_r + 2z\boldsymbol{i}_z)$ (where G is the strain rate), with the dynamic pressure equal to zero. The strain rate, G, is assumed to be small enough that the creeping-motion approximation can be applied; i.e. the Reynolds number, Re, satisfies

$$Re = \frac{\rho G a^2}{\mu} \ll 1.$$

Thus, the equations of motion are linear. The problem remains nonlinear through the boundary conditions, however, because the interface shape, the sphere position $z = -h$, and the position of the contact line ϕ, all remain unknown.

An excellent method of solution for this type of free boundary problem is the boundary-integral method used extensively in our group, cf. Geller, Lee & Leal (1986), Lee & Leal (1982), Chi & Leal (1987), Stone & Leal (1987), following earlier work by Youngren & Acrivos (1975, 1976), Rallison & Acrivos (1987), and others. We refer the reader to these earlier papers for many of the details.

In the present problem, we non-dimensionalize using the characteristic velocity

Ga, length a and stress $G\mu$. The creeping-motion equations in the lower fluid can thus be expressed in the form

$$\left.\begin{aligned} 0 &= -\nabla p + \nabla^2 \boldsymbol{u} \\ 0 &= \nabla \cdot \boldsymbol{u}. \end{aligned}\right\} \tag{1}$$

In addition to the condition stated previously at large distances from the particle, the boundary conditions at the interface are

$$\boldsymbol{u} \cdot \boldsymbol{n} = 0, \tag{2}$$

$$\boldsymbol{n} \cdot \boldsymbol{T} = \frac{1}{Ca}(\nabla \cdot \boldsymbol{n})\,\boldsymbol{n} - \frac{1}{Cg} f \boldsymbol{n}, \tag{3}$$

and at the particle surface

$$\boldsymbol{u}_{\mathrm{p}} = 0. \tag{4}$$

The parameters which appear in the condition (3) are the capillary number, $Ca \equiv \mu Ga/\sigma$, and the ratio of capillary number to Bond number, $Cg \equiv \mu G/ag$. In addition, the steady-state solution must satisfy the macroscopic condition of zero net force on the particle in the z-direction (this condition is satisfied trivially in the r-direction owing to symmetry), i.e.

$$F_z = 0, \tag{5a}$$

where

$$\begin{aligned} F_z = &-\left(\tfrac{4}{3}\pi \frac{\rho_{\mathrm{p}}}{\rho} - \pi h \sin^2\phi + \tfrac{2}{3}\pi(-1+\cos^3\phi)\right)\frac{1}{Cg} - 2\pi \sin\phi \sin(\phi+\theta_{\mathrm{c}})\frac{1}{Ca} \\ &+ 2\pi \int_{\pi-\phi}^{\pi} T^{\mathrm{P}}_{nz} \sin\theta \,\mathrm{d}\theta \\ &= F_{\mathrm{buoy}} + F_{Ca} + F_{\mathrm{visc}}. \end{aligned} \tag{5b}$$

The three terms which appear in (5b) are, from left to right, the net buoyancy force, the z-component of the capillary force at the contact line, and the hydrodynamic force due to the fluid motion. The parameters Ca and Cg appear in the first two terms because the force has been non-dimensionalized with the characteristic viscous force, μGa^2, in order to be consistent with the characteristic stress, μG, which was used in (1)–(3). Here, as in Lee & Leal (1982), the interface shape is represented by $z = f(r)$, and the outward-pointing normal at the interface is $n \equiv \Delta H/|\Delta H|$ where $H = z - f(r)$. Finally, the interface must approach the particle surface with the prescribed macroscopic contact angle, θ_{c}.

In addition to Ca and Cg, the only dimensionless parameter that appears in (1)–(5) is the ratio of particle to fluid densities, ρ_{p}/ρ. It will be noted that Ca and Cg both appear twice, in the normal stress condition (3) and the macroscopic force balance (5). The parameter Ca provides a measure of the ratio of characteristic viscous to capillary forces, and, in the present problem, this appears both in the ratio of viscous forces in the fluid that tend to pull the particle from the interface to interfacial tension forces which tend to hold the particle on the interface, and also as the ratio of viscous forces tending to deform the interface relative to capillary forces which resist interface deformation. Likewise, Cg is the ratio of these viscous forces in the fluid to body forces that tend to pull the particle from the interface, and also the ratio of viscous forces to body forces which tend to resist interface deformation. The ratio $(Ca/Cg)^{\frac{1}{2}}$ can be viewed as a dimensionless particle radius scaled with an intrinsic measure of the interface curvature, i.e. $a(\sigma/\rho g)^{-\frac{1}{2}}$, and this quantity is used frequently in the statics problem.

In the present work, we concentrate primarily upon the limiting case of neutrally buoyant particles, $\rho_{\mathrm{p}}/\rho = 1$. It may be noted that there will always be an equilibrium

solution to the statics problem for $\rho = \rho_p$, cf. Boucher & Jones (1981). Thus, if a flow problem for $\rho_p = \rho$ is found to have no solution, this must be due solely to the presence of the flow.

The problem, then, is to determine the positions of the sphere centre, $-h$, and the contact line, ϕ, together with the shape of the interface $f(r)$ such that the force balance on the sphere is satisfied, the normal velocity on the interface is zero, and the angle of the interface at the contact line agrees with the specified macroscopic contact angle, θ_c.

3. Solution methodology

In the present work, the problem outlined above is solved via the boundary-integral method, for several values of θ_c and a range of values of Ca and Cg. The boundary-integral method for an unbounded domain requires that the flow variables decay to zero at infinity. Therefore, the velocity and stress are written in terms of disturbance variables, as in Rallison & Acrivos (1978), where $\boldsymbol{u}' \equiv \boldsymbol{u} - \boldsymbol{u}^\infty$ is the disturbance velocity and $\boldsymbol{T}' \equiv \boldsymbol{T} - \boldsymbol{T}^\infty$ is the disturbance stress. Ladyzhenskaya's (1969) general solution for the disturbance velocity and disturbance pressure at any point in the fluid $\boldsymbol{x}$ is

$$\boldsymbol{u}'(\boldsymbol{x}) = \frac{1}{8\pi}\int_S \left(\frac{\boldsymbol{I}}{R} + \frac{(\boldsymbol{x}-\boldsymbol{\eta})(\boldsymbol{x}-\boldsymbol{\eta})}{R^3}\right)\cdot \boldsymbol{T}'(\eta)\cdot \boldsymbol{n}\,\mathrm{d}S_\eta - \frac{3}{4\pi}\int_S \frac{(\boldsymbol{x}-\boldsymbol{\eta})(\boldsymbol{x}-\boldsymbol{\eta})}{R^5}\cdot \boldsymbol{u}'(\eta)\cdot \boldsymbol{n}\,\mathrm{d}S_\eta, \quad (6)$$

$$p'(\boldsymbol{x}) = \frac{1}{2\pi}\int_S \left(\frac{\boldsymbol{I}}{R} - \frac{3(\boldsymbol{x}-\boldsymbol{\eta})(\boldsymbol{x}-\boldsymbol{\eta})}{R^5}\right)\cdot \boldsymbol{u}'(\eta)\cdot \boldsymbol{n}\,\mathrm{d}S_\eta + \frac{1}{4\pi}\int_S \frac{(\boldsymbol{x}-\boldsymbol{\eta})}{R^3}\cdot \boldsymbol{T}'(\eta)\cdot \boldsymbol{n}\,\mathrm{d}S_\eta. \quad (7)$$

Because the pressure associated with the undisturbed flow at infinity undergoes a jump across the interface $p_\infty - p_{\infty g} = 4G\mu$ (where p_∞ and $p_{\infty g}$ are the constant pressures in the lower fluid and the gas associated with the flow at infinity), the disturbance pressures are defined as $p'_g \equiv p_g$ and $p' = p - 4G\mu$ or, in dimensionless terms, $p' = p - 4$ so that $p'_g, p' \to 0$ as $|\boldsymbol{x}| \to \infty$.

The details of the derivation of the system of boundary-integral equations from (6) and (7) are similar to those of Lee & Leal (1982), but with additional terms in the equations due to the flow at infinity. After applying the double-layer jump condition, and boundary condition (2), the velocity on the interface in the limit as $\boldsymbol{x} \to \boldsymbol{S}_I$ from the lower fluid is given by

$$\tfrac{1}{2}\boldsymbol{u}^I(\boldsymbol{x}) = -\frac{3}{4\pi}\int\left(\frac{\boldsymbol{rrr}}{R^5}\right)\cdot \boldsymbol{u}^I\cdot \boldsymbol{n}\,\mathrm{d}S_I + \frac{1}{8\pi}\int\left(\frac{\boldsymbol{I}}{R} + \frac{\boldsymbol{rr}}{R^3}\right)\cdot \boldsymbol{T}^I\cdot \boldsymbol{n}\,\mathrm{d}S_I$$

$$+\frac{1}{8\pi}\int\left(\frac{\boldsymbol{I}}{R} + \frac{\boldsymbol{rr}}{R^3}\right)\cdot \boldsymbol{T}^P\cdot \boldsymbol{n}\,\mathrm{d}S_P + \frac{3}{4\pi}\int\left(\frac{\boldsymbol{rrr}}{R^5}\right)\cdot \boldsymbol{u}_\infty\cdot \boldsymbol{n}\,\mathrm{d}S_P - \frac{1}{8\pi}\int\left(\frac{\boldsymbol{I}}{R} + \frac{\boldsymbol{rr}}{R^3}\right)\cdot \boldsymbol{T}^P_\infty\cdot \boldsymbol{n}\,\mathrm{d}S_P. \quad (8)$$

Here, we denote the particle surface as S_P and the interface surface as S_I. In addition, we introduce the shortened notation $\boldsymbol{r} \equiv \boldsymbol{x} - \boldsymbol{\eta}$. The velocity on the sphere surface

satisfies condition (4). Thus, when (6) is applied at the sphere surface, and the double-layer jump condition is used, we obtain

$$\begin{aligned}\mathbf{0} = &-\frac{3}{4\pi}\int\left(\frac{\boldsymbol{rrr}}{R^5}\right)\cdot\boldsymbol{u}^{\mathrm{I}'}\cdot\boldsymbol{n}\,\mathrm{d}S_{\mathrm{I}}+\frac{1}{8\pi}\int\left(\frac{\boldsymbol{I}}{R}+\frac{\boldsymbol{rr}}{R^3}\right)\cdot\boldsymbol{T}^{\mathrm{I}'}\cdot\boldsymbol{n}\,\mathrm{d}S_{\mathrm{I}}\\ &+\frac{1}{8\pi}\int\left(\frac{\boldsymbol{I}}{R}+\frac{\boldsymbol{rr}}{R^3}\right)\cdot\boldsymbol{T}^{\mathrm{P}}\cdot\boldsymbol{n}\,\mathrm{d}S_{\mathrm{P}}+\tfrac{1}{2}\boldsymbol{u}_\infty\\ &+\frac{3}{4\pi}\int\left(\frac{\boldsymbol{rrr}}{R^5}\right)\cdot\boldsymbol{u}_\infty\cdot\boldsymbol{n}\,\mathrm{d}S_{\mathrm{P}}-\frac{1}{8\pi}\int\left(\frac{\boldsymbol{I}}{R}+\frac{\boldsymbol{rr}}{R^3}\right)\cdot\boldsymbol{T}^{\mathrm{P}}_\infty\cdot\boldsymbol{n}\,\mathrm{d}S_{\mathrm{P}}. \qquad (9)\end{aligned}$$

The disturbance stress on the interface, defined as $\boldsymbol{n}\cdot\boldsymbol{T}^{\mathrm{I}'}\equiv\boldsymbol{n}\cdot\boldsymbol{T}^{\mathrm{I}}-\boldsymbol{n}\cdot\boldsymbol{T}^{\mathrm{I}}_\infty$, can be evaluated from the interface shape via (3) and the form of the stress contribution from the undisturbed flow at infinity,

$$\boldsymbol{n}\cdot\boldsymbol{T}_\infty=\boldsymbol{n}\cdot(-p_2\boldsymbol{I}+(-2\boldsymbol{i}_r\boldsymbol{i}_r+4\boldsymbol{i}_z\boldsymbol{i}_z))=-6n_r\boldsymbol{i}_r.$$

Here, as mentioned previously, the constant dynamic pressure associated with the undisturbed flow has been chosen to balance the viscous stress of the undisturbed flow. In addition to $\boldsymbol{T}^{\mathrm{I}'}$, the velocity and stress contributions $\boldsymbol{u}_\infty$ and $\boldsymbol{T}^{\mathrm{P}}_\infty$ associated with the undisturbed flow are known. Thus, for a given interface and sphere configuration, i.e. $f(r)$, h and ϕ, (8) and (9) can be solved simultaneously to determine the disturbance velocity on the interface and the net stress on the particle surface. The problem then, is to determine the configuration, i.e. $f(r)$, h and ϕ, such that the boundary condition (2) and the macroscopic force balance (5) are satisfied for a given set of values of Ca, Cg and θ_{c}.

The method used to solve (8) and (9), for a given configuration, is essentially the same collocation scheme described by Geller *et al.* (1986). The surface integrals in (8) and (9) are first reduced to line integrals by integrating analytically over the azimuthal angle, for this axisymmetric problem. The infinite boundary is then truncated at some large but finite radius, R_0, and subdivided, along with the portion of the particle surface that is exposed to the lower fluid, into N_{I} and N_{P} small segments, respectively. The number of segments varied between 25 and 35 unequal-sized segments for N_{I}, with the highest concentration of segments being near the particle where the interface deformation is largest, and 20 and 25 segments for N_{P}, which were spaced evenly except very near the contact line where additional segments were added. These additional segments are necessary to achieve a reasonable approximation of the shear stress distribution in the vicinity of the contact line, which exhibits a weak singularity $O(r^{-m})$ with $m\leqslant\frac{1}{2}$ for $0\leqslant\theta_{\mathrm{c}}\leqslant\frac{1}{2}\pi$, cf. Moffatt (1964). In the present work, the unknown basis functions for the velocity and stress were assumed to vary linearly over the boundary segments. Alternatively, the same degree of accuracy could also be achieved by increasing the number of boundary elements and assuming the basis functions to be constant over the elements. However, the use of linear basis functions was found to be numerically faster because the integrals required for the linear weighting functions are no more difficult to evaluate than the corresponding integrals with constant weighting functions, and the size of the matrix that must be inverted is smaller. Vector equation (8) is evaluated at the N_{I} interface interval centres, and vector equation (9) is evaluated at the N_{P} particle interval centres, thus generating a system of $2N_{\mathrm{I}}+2N_{\mathrm{P}}$ linear algebraic equations (Kantorovich & Krylov 1958). For a given configuration

($f(r)$, h and ϕ) these equations are solved for the $2N_{\mathrm{I}}+2N_{\mathrm{P}}$ unknowns; $u_r'(N_{\mathrm{I}})$, $u_z'(N_{\mathrm{I}})$, $T_{nr}^{\mathrm{P}}(N_{\mathrm{P}})$, and $T_{nz}^{\mathrm{P}}(N_{\mathrm{P}})$. The normal vector to the interface and the local interface curvature, which appears in the integrands through the use of boundary condition (3), are evaluated using a cubic spline to represent the interface shape as $f(r)$. The final line integrals, obtained after carrying out the azimuthal integration (Lee & Leal 1982), are evaluated numerically using a seven-point Gauss quadrature and the accuracy is checked by comparing to an eleven-point Gauss quadrature. In doing this integration, a small line element is cut out around the singular point and evaluated analytically. In addition, the accuracy is improved further by subdividing the main segment into smaller segments near the singular points.

In general, with Ca, Cg and θ_{c} specified, the solutions for the interface velocities and the stress on the sphere will not satisfy boundary condition (2) nor the force balance (5), and the interface/particle configuration $f(r)$, h and ϕ must be modified. Initially, attempts were made to modify the interface shape and particle position via an explicit, pseudo-time-dependent iteration, in which the positions of node points on the interface were stepped proportional to the calculated values for $\boldsymbol{u}^{\mathrm{I}}\cdot\boldsymbol{n}$, and the position of the particle was incremented according to the imbalance in total force, from the sum of the three terms in (5). However, all such explicit iterative schemes were found to be slow and prone to numerical instability, leading to kinks in the interface shape and rapid divergence of the entire solution. Use of implicit time-stepping schemes stabilizes the system somewhat but still result in very long computation times and occasional instabilities in the solutions.

Thus, to speed convergence, to provide a more stable means of obtaining equilibrium solutions, and to better determine when no solutions exist, a modified Newton's scheme is used to obtain subsequent values of $f(r)$, h and ϕ. This scheme is similar to that first used by Youngren & Acrivos (1976). It should be noted that the contact point (line) was not included as a node point in the approximation scheme. However, the first few node points on the interface and on the sphere surface were concentrated very near the contact point and a two-point right-handed difference scheme (see Appendix A) was used to set the position of the contact point to ensure that the contact angle has the specific value, to within an accuracy of 10^{-4}. Unlike the problem considered by Youngren & Acrivos (1976), the occurrence of neutral eigenvalue solutions does not cause difficulties in this study since the presence of the sphere boundary modifies the linear system. However, as already found by Youngren & Acrivos (1976), the radius of convergence of Newton's scheme in this problem is not very large. This is a consequence of the fact that we use only a partial Newton scheme rather than a global Newton iteration in which the whole problem is incremented simultaneously at each step. (We are currently in the process of developing such a global Newton's algorithm.) Therefore, a good initial guess for the interface shape and sphere position is required, and in this study the static configuration is generally used as a first guess for the interface shape and particle position, with correspondingly small initial values of Ca and Cg. This static shape is calculated using a slight modification of the method of Rapacchietta & Neumann (1977) (see Appendix B). At each step in the iteration, the normal velocity can be calculated at the N_{I} interface node points, and the net force on the particle can be determined by solving (8) and (9) and evaluating (5b). For convenience, let us define the vector x_j

$$x_j = \begin{cases} (\boldsymbol{u}\cdot\boldsymbol{n})_j & \text{if } j \leqslant N_{\mathrm{I}}; \\ F_{\mathrm{net}} & \text{if } j = N_{\mathrm{I}}+1, \end{cases} \tag{10}$$

which thus represents the deviation of the system from equilibrium (at equilibrium all the elements of x_j would be zero). Similarly, the vector z_j

$$z_j = \begin{cases} f_j & \text{if} \quad j \leqslant N_{\mathrm{I}}; \\ h & \text{if} \quad j = N_{\mathrm{I}}+1 \end{cases} \tag{11}$$

represents the interface shape at each r_j and the particle position. The Jacobian matrix, $\partial x_i/\partial z_j$, that is required for the Newton scheme is evaluated numerically by perturbing in turn each of the node points $f(N_{\mathrm{I}})$ and the sphere position h, and calculating the new N_{I} normal velocities and the new net force on the particle. This Jacobian has elements

$$A_{ij} = \begin{cases} \dfrac{\Delta(\boldsymbol{u}\cdot\boldsymbol{n})_i}{\Delta f_j} & \text{if} \quad i,j \leqslant N_{\mathrm{I}}; \\ \dfrac{\Delta(\boldsymbol{u}\cdot\boldsymbol{n})_i}{\Delta h} & \text{if} \quad i \leqslant N_{\mathrm{I}}, j \geqslant N_{\mathrm{I}}+1; \\ \dfrac{\Delta F_{\mathrm{net}}}{\Delta f_j} & \text{if} \quad i = N_{\mathrm{I}}+1, j \leqslant N_{\mathrm{I}}; \\ \dfrac{\Delta F_{\mathrm{net}}}{\Delta h} & \text{if} \quad i = N_{\mathrm{I}}+1, j = N_{\mathrm{I}}+1. \end{cases} \tag{12}$$

Given A_{ij}, a new interface shape and particle position is calculated according to

$$z_j^{n+1} = z_j^n - wA_{ij}^{n^{-1}} x_j^n, \tag{13}$$

so that the N_{I} normal velocities on the interface and the net force on the particle are driven towards zero. It should be noted that we have followed Youngren & Acrivos (1976) and used under-relaxation in this calculation of shape change with a relaxation factor $w \leqslant 1$, which is chosen so that the maximum increment in shape is bounded by a specified limit. The use of $w < 1$ prevents divergence of the solution.

The Jacobian changes very little over the course of convergence for a particular choice of parameters Ca, Cg and θ_{c}, and a sufficiently close starting configuration. Thus, the Jacobian is not updated unless convergence is unusually slow, and the solution scheme is more accurately described as a Picard iteration rather than a 'modified' Newton scheme. The interface shape and sphere position is iterated until conditions (2) and (5) are satisfied to at least 10^{-4} in each normal velocity component and the net force. It will be noted that each iteration requires solution of the boundary-integral problem to determine x_j, even though the elements of the Jacobian are not changed. When the conditions (2) and (5) are satisfied, a measure of the change in shape at the $(n+1)$th iteration, as defined by Youngren & Acrivos (1976), $W = (z_j^{n+1}-z_j^n)(z_j^{n+1}-z_j^n)/w$ is always less than 10^{-10}, i.e. the configuration simultaneously reaches a steady state.

In many of the cases studied, the parameters Ca and Cg were increased, with the ratio, Ca/Cg, fixed, which is representative of the physical situation where the flow strength is increased, and the particle size (or ratio Ca/Cg) and fluid properties are held fixed. Changes in the flow strength would occur in the flotation problem through changes in the size of the collector bubble. We have also considered some cases in which Cg was held fixed while Ca was increased, which is representative of the physical situation where the flow strength, particle size and fluid densities are held fixed, while the surface tension is decreased, possibly owing to the addition of a surfactant. The third possibility, of holding Ca fixed and varying Cg, was not

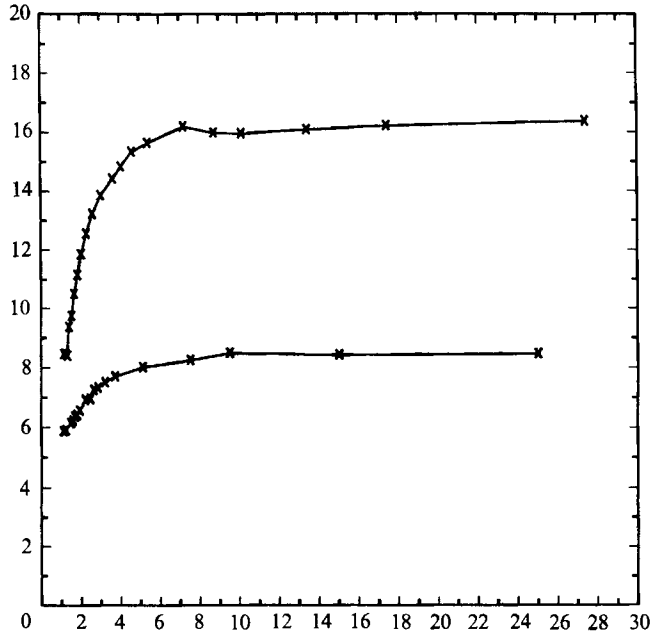

FIGURE 2. Viscous drag on sphere as a function of interface truncation for $\rho_p = \rho$: $\theta_c = \frac{1}{2}\pi$, $Ca = 0.1$, $Cg = 0.05$; $\theta_c = \frac{8}{9}\pi$, $Cg = Ca = 0.05$.

explored because it corresponds to variation in the liquid density for a system with constant surface tension and flow strength, and thus would not be realized in any straightforward way in a flotation process.

For all of these investigations, after varying the parameters, a new Jacobian is calculated and the entire procedure is repeated until the solution has converged to a new steady shape satisfying the force balance on the particle and having the required macroscopic contact angle. Convergence of the interface shape is not obtained unless a sufficient number of segments on the interface are used, since the errors in calculating the interface curvature are very sensitive to the spatial resolution. However, even for the most deformed interface we consider, the final steady-state configuration is not affected by the number of intervals for N_I greater than 25. Also, in some instances convergence is accelerated by using a different (smaller) relaxation factor for the net force on the particle than for the normal velocities on the interface. This indicates, as might be expected, that the solution is more sensitive to variations in the particle position than to variations in the interface shape.

Finally, it should be recognized that steady-state solutions may exist only for a limited range of Ca and Cg for a system with any fixed contact angle θ_c. In particular, if we follow one of the parameter pathways that was described above beginning with the static limit $Ca = Cg = 0$, we will see that we reach a limit point for the particular branch of steady-state solutions. For larger values of Ca (for Cg = constant = 0, or $Ca = Cg$), a steady solution of this family does not exist, and we identify the limit point as *the critical condition for loss of capture stability*. In order to explore the solution behaviour in the vicinity of this limit point, where the configuration becomes increasingly sensitive to variations in Ca, it is necessary to use a 'continuation method', cf. Kubicek & Marek (1983). In this procedure, we adopt the

sphere position, h, as the independent parameter, and calculate the capillary number corresponding to a particular value of h as part of the solution. Thus, a new Jacobian is calculated as in (12), but with h replaced everywhere by Ca as an unknown. The dependence on Cg is included implicitly through the stress and force balances. In this way, we can easily achieve solutions for Ca values arbitrarily close to the critical capillary number, as well as exploring the nature of the limit point (for example, we can examine the unstable branch of steady solutions which emanates from the limit point in Ca).

The effects of truncating the interface at R_0 are shown in figure 2, where the viscous drag on the particle at steady state is plotted versus R_0 for the parameters $\theta_c = \frac{1}{2}\pi$, $Ca = 0.1$, $Cg = 0.05$ and $\theta_c = \frac{8}{9}\pi$, $Ca = Cg = 0.05$. The viscous drag is seen to be relatively constant for truncation distances R_0 greater than 10 particle radii. Since the meniscus depression, h, is generally $O(1)$, a truncation distance of 15 is used in all the calculations that are reported below.

4. Results

We begin by considering neutrally buoyant particles, i.e. $\rho_p/\rho = 1$, which will form the primary focus of our investigation. In this case, steady-state configurations were determined for contact angles of $\theta_c = \frac{8}{9}\pi$, where the fluid does not preferentially wet the particle (representative of a hydrophobic particle which should be readily floated), $\theta_c = \frac{1}{2}\pi$ where the fluid is intermediate between wetting and non-wetting the particle, and $\theta_c = \frac{1}{4}\pi$ where the fluid preferentially wets the particle (representative of a hydrophylic particle which should not be readily floated). Solutions were also sought for $\theta_c = \frac{1}{9}\pi$ (a fluid which wets the particle even more strongly), but it is advantageous to delay discussion of this case until we have presented and discussed our results for the other, more moderate values of θ_c. For the solutions that are presented below, $\theta_c = \frac{1}{4}\pi$, $\frac{1}{2}\pi$ and $\frac{8}{9}\pi$, the capillary number is increased either with the constraint $Ca = Cg$, or with Cg = constant, as indicated in the preceeding section.

4.1. *Neutrally buoyant particles with $Ca = Cg$ and a small contact angle*

The effect of flow on the steady-state particle–interface configuration is first discussed for a relatively small contact angle, $\theta_c = \frac{1}{4}\pi$. In this case, for $Ca = Cg$, steady-state solutions were found up to a maximum value of $Ca = Cg$ of 0.0327. Interface contours corresponding to these steady-state solutions are shown in figure 3. For simplicity of presentation, these contours are plotted relative to a coordinate system that is fixed at the centre of the particle. The absolute position of the particle centre can be determined from its position relative to the plane of the flat, undisturbed part of the interface. Interface configurations which correspond to *stable* steady-state solutions are shown as solid contours. *Unstable* steady solutions are shown as dashed contours. The transition between stable and unstable steady solutions occurs at a limit point for the branch of steady solutions that emanates from the origin, i.e. $Ca = Cg = 0$. This limit point occurs at the critical value of $Ca\,(= Cg)$ for loss of capture stability; in this case $Ca_c\,(= Cg) = 0.0327$.

To discuss the nature of the solution in the vicinity of the limit point, it is useful to consider the mechanisms by which the system attempts to accommodate an increase in the flow strength (i.e. an increase in $Ca = Cg$). For this purpose, it is informative to examine the details of changes in the particle–interface configuration and especially to consider how the three force contributions (i.e. buoyancy, capillary, and hydrodynamic) vary with changes in the configuration as Ca is gradually

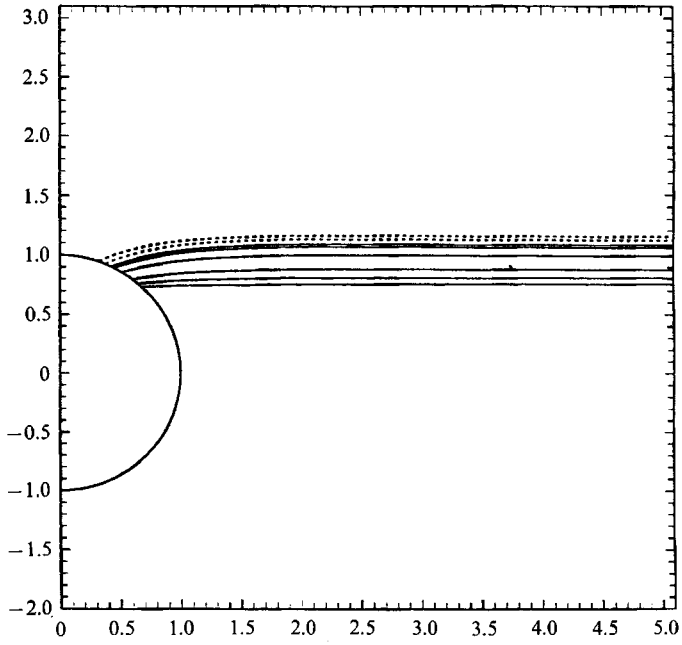

FIGURE 3. Equilibrium sphere/interface configuration for: $\theta_c = \frac{1}{4}\pi$, $\rho_p = \rho$: ——, $Cg = Ca = 0$, 0.01, 0.02, 0.03, 0.0325, 0.0327 (stable); ------, $Cg = Ca = 0.0320$, 0.0300 (unstable).

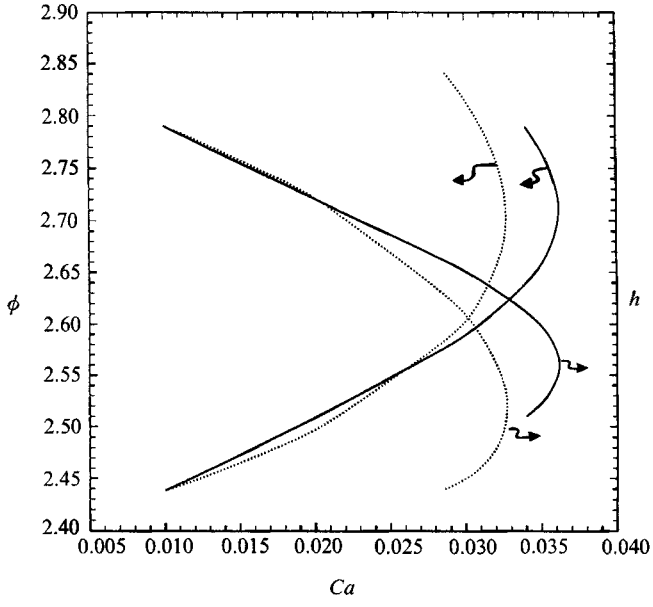

FIGURE 4. Sphere position, h, and contact line position, ϕ, as a function of capillary number for $\theta_c = \frac{1}{4}\pi$, $\rho_p = \rho$: ——, $Cg = 0.01$; · · · · · ·, $Cg = Ca$.

increased. Examining figure 3, we see that as the flow strength increases, the interface curvature increases and the contact line moves closer to the top of the particle. Indeed, as we continue to increase Ca (restricting our discussion to the stable solutions for the moment), it is evident that the particle–interface configuration becomes more and more sensitive to small increases in Ca as we

approach the final stable steady-state solution (the limit point). This effect is seen clearly in figure 4 where the equilibrium particle position, $+h$, and the contact line position, ϕ, are plotted as a function of the capillary number. As the 'critical' capillary number is approached ($Ca = Cg = 0.0327$), the solution exhibits the 'classical' limit-point behaviour. It is not surprising to note that there is actually a second steady (but unstable) solution possible for Ca in the vicinity of Ca_c, which we have obtained by means of the continuation method that was described in the preceding section. The corresponding interface configurations are shown as the dashed contours in figure 3.

The presence of a limit point, of the type illustrated in figure 4, means that the system undergoes a change in stability from stable solutions for smaller ϕ and less negative $-h$) to unstable solutions for larger ϕ (and more negative $-h$). Indeed, this change of stability may be thought of as being physically reponsible for existence of the limit point. In order to understand this change from stable to unstable configurations with increase of ϕ or $|h|$, it is necessary to examine the changes in the various contributions to the force balance on the sphere, equation (5*b*), as Ca is increased. It should be noted, however, that the behaviour of (5*b*) appears unphysical for $Ca \ll 1$. The problem is that the forces in (5*b*) are non-dimensionalized using the characteristic viscous scale $\mu G a^2$, and this scale factor is zero in the static (no-flow) limit. Hence, the magnitudes of the non-dimensionalized buoyant and capillary force terms, which are measured relative to this viscous scale, both blow up in the limit, $Ca = Cg \to 0$. In order to discuss the behaviour of the force balance on the particle with variation in $Ca = Cg$, on the solution branch which includes the static limit, it is necessary to non-dimensionalize (5*b*) using the characteristic magnitude of either the capillary or buoyancy force. We choose the buoyancy force, and obtain the corresponding form of (5*b*) by multiplying through by Cg, i.e.

$$F_z^* = -\left(\tfrac{4}{3}\pi\frac{\rho_p}{\rho} - \pi h\sin^2\phi + \tfrac{2}{3}\pi(-1+\cos^3\phi)\right) - 2\pi\sin\phi\sin(\phi+\theta_c)\frac{Cg}{Ca} + 2\pi Cg\int_{\pi-\phi}^{\pi} T^p_{nz}\sin\theta\,\mathrm{d}\theta. \quad (14)$$

This corresponds to non-dimensionalizing the force with respect to $F_c = a^3\rho g$.

With the rescaling that is inherent in (14), the behaviour of the three force components with increase of $Ca = Cg$ is most easily envisioned as corresponding to an increase in G with fixed material properties. In particular, as Ca is increased with $Ca/Cg = 1$, it can be seen from (14) that both the buoyancy and capillary forces remain $O(1)$, while the viscous term increases in proportion to Ca. The other situation, considered below, where Ca is increased with Cg fixed, is most easily envisioned as corresponding to a decrease in σ for constant flow strength μG in a system with fixed ρ and a. In this case, as Ca is increased, the magnitude of the buoyancy and viscous contributions remain $O(1)$, while the capillary forces decrease as Ca^{-1}.

In figure 5 we have plotted the three contributions to the force on the sphere for the case $\theta_c = \frac{1}{4}\pi$, $Ca = Cg$, that was shown in figures 3 and 4. In the static limit, the viscous force is zero and there is a precise balance between the buoyancy and capillary forces. However, as Ca increases, the viscous force increases and, in response, the particle is displaced further from the plane of the undeformed interface and the contact line moves toward the top of the sphere. The effect of this change can be seen in figure 5 to result in an increase in the capillary force, as well as a decrease

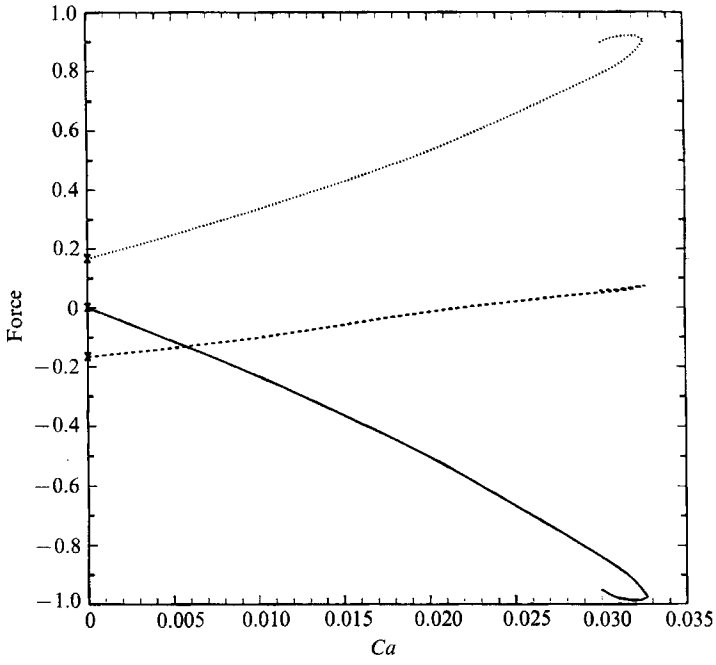

FIGURE 5. Components of net force on sphere as a function of capillary number for $\theta_c = \frac{1}{4}\pi$, $\rho_p = \rho$, $Cg = Ca$: ——, viscous drag; ------, net buoyancy force; · · · · · ·, capillary force.

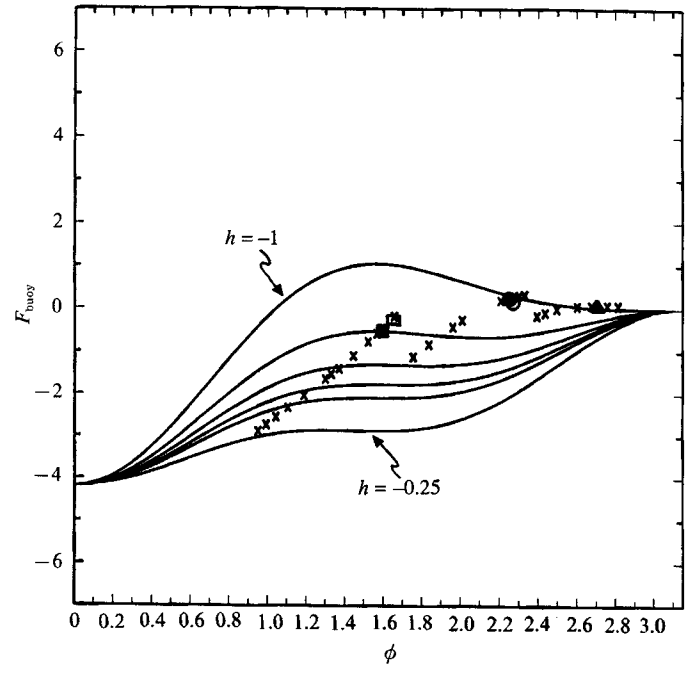

FIGURE 6. Net buoyancy force for $\rho_p/\rho = 1$ as a function of contact line position for sphere displacements $h = -1.0$, -0.5, -0.25, -0.1, 0, 0.25. The trajectories in terms of (h, ϕ) for fixed values of the contact angle (θ_c) and increasing values of $Ca = Cg$ are shown by the symbol × for the three cases $\theta_c = \frac{8}{9}\pi$ (left), $\theta_c = \frac{1}{2}\pi$ (centre), and $\theta_c = \frac{1}{4}\pi$ (right). The critical points for loss of capture stability are shown via the symbols: ▲, $\theta_c = \frac{1}{4}\pi$, $Ca = Cg$; △, $\theta_c = \frac{1}{4}\pi$, $Cg = 0.01$; ●, $\theta_c = \frac{1}{2}\pi$, $Ca = Cg$; ○, $\theta_c = \frac{1}{2}\pi$, $Ca = 0.05$; ■, $\theta_c = \frac{8}{9}\pi$, $Ca = Cg$; □, $\theta_c = \frac{8}{9}\pi$, $Cg = 0.05$.

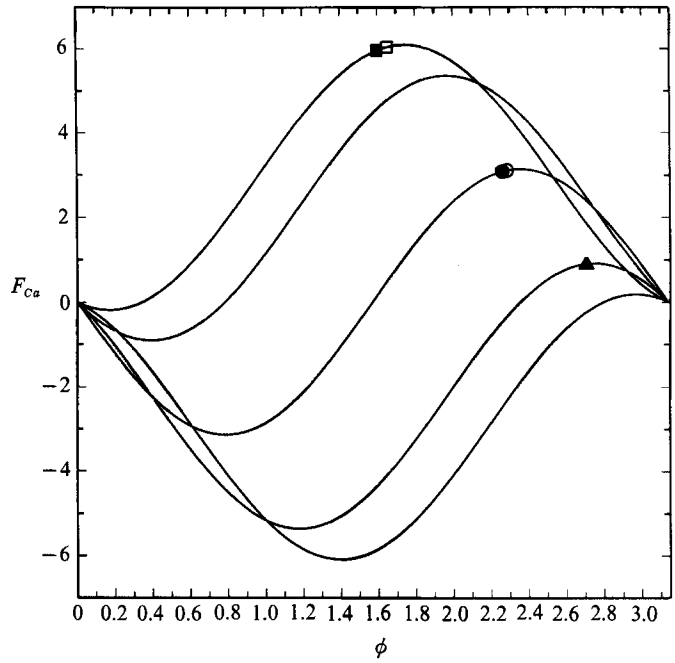

FIGURE 7. Capillary force as a function of contact line position for contact angles $\theta_c = \frac{1}{8}\pi, \frac{1}{4}\pi, \frac{1}{2}\pi, \frac{3}{4}\pi, \frac{8}{9}\pi$; contact line position at which critical capillary number occurs for: $\theta_c = \frac{1}{4}\pi$, $Cg = Ca$ (▲), $Cg = 0.01$ (△); $\theta_c = \frac{1}{2}\pi$, $Cg = Ca$ (●), $Cg = 0.05$ (○); $\theta_c = \frac{8}{9}\pi$, $Cg = Ca$ (■), $Cg = 0.05$ □).

in the magnitude of the net buoyancy force which is tending to pull the particle from the interface. Both of these changes act to compensate for the large increase in the magnitude of the viscous force with increase of Ca.

The buoyancy force for fixed ρ_p/ρ can be seen from (14) to depend only on the configuration represented by h and ϕ. The details of this force for $\rho_p/\rho = 1$ are shown in figure 6 where we plot F_{buoy} *vs.* ϕ for several fixed values of sphere position h. The result represents a complicated interplay between the weight of the portion of the sphere above the interface (i.e. above the contact line) and the meniscus depression which tends to compensate by increasing the hydrostatic pressure on the submerged portion of the sphere. It is difficult to draw any general conclusions about the expected behaviour of F_{buoy} with changes in Ca, because any such change is accompanied by simultaneous changes in h and ϕ. However, for small contact angles such as $\theta_c = \frac{1}{4}\pi$, the neutrally buoyant sphere is almost completely submerged in the lower fluid, even for the static limit, and the magnitude of the net buoyancy force is small for all accessible values of $Ca = Cg$ (note, from figure 6, that the buoyancy force is precisely zero for all h in the limit $\phi \to \pi$, where the sphere is completely submerged). Trajectories, in terms of changes in h and ϕ with increase of $Ca = Cg$, illustrated in figure 6 by the symbol × (see caption) for $\theta_c = \frac{1}{4}\pi, \frac{1}{2}\pi$ and $\frac{8}{9}\pi$ respectively. Clearly, since ϕ is quite large even for $Ca = Cg = 0$, there is little latitude for anything but the small monotonic increase in F_{buoy} toward zero that was shown in figure 5.

The capillary force for a given θ_c can be seen from (14) to depend only on the position ϕ of the contact line. This dependence on ϕ is illustrated in figure 7 for several fixed values of θ_c, including the case $\theta_c = \frac{1}{4}\pi$ that was considered above. In general (i.e. for arbitrary θ_c), the capillary force is negative for small ϕ (reflecting the

direction of action of the force for fixed $\theta_c \neq \pi$), becomes positive at some particular values of ϕ where the z-component of the tangent to the interface at the contact line changes from negative to positive, and then continues to increase with increase in ϕ as the direction of action of the capillary force at the contact line becomes increasingly oriented in the positive z-direction. Beyond $\phi = \frac{1}{2}\pi$, however, the contact line begins to decrease in length and, in addition, for $\theta_c > \frac{1}{2}\pi$, there will be a value of ϕ, $\frac{1}{2}\pi < \phi < \pi$, where the tangent plane to the interface passes through the vertical, and the direction of action of the capillary force again begins to deviate increasingly from vertical. As a result of these two factors, the capillary force must eventually pass through a maximum and begin to decrease toward zero at $\phi = \pi$ for all θ_c.

With the understanding gained from our examination of the buoyancy and capillary forces in figures 5, 6 and 7, we can now understand the existence of the limit point which appeared in the case $\theta_c = \frac{1}{4}\pi$ (cf. figures 3, 4 or 5) for $Ca = Cg = 0.0327$. In particular, since θ_c is small, there is only a small range of values of ϕ where the capillary force acts in the positive z-direction. Clearly, if a steady-state configuration exists for some Ca, it must occur for this range of ϕ values so that the capillary force can balance the buoyancy and viscous forces which both act in the opposite direction. However, since the requirement for an upwardly directed capillary force restricts ϕ to values relatively close to π, buoyancy forces must remain quite small for all Ca where steady solutions exist, and the increase in viscous forces resulting from the increase in Ca must be balanced primarily by increases in the capillary force associated with increases in ϕ. At $Ca = 0.0327$, however, we reach the peak in the capillary force as a function of ϕ and any further increase in Ca (i.e. the viscous force) cannot be accommodated. Indeed, it can be seen from figure 7 that the contact line position corresponding to the limit point in figure 3 or 4 coincides very closely with the maximum positive capillary force.

Additional steady solutions for larger ϕ, shown as the dashed contours in figure 3, can only exist for $Ca < 0.0327$ where the viscous force is smaller. Of course, it is known from general mathematical analyses of limit-point behaviour that this continuation branch of solutions must be unstable (Iooss & Joseph 1980). From a physical point of view, this instability is a consequence of the fact that any infinitesimal increase in ϕ (due, for example, to an infinitesimal fluctuation in the hydrodynamic force) results in a decrease in the capillary 'restoring' force and an increase in the viscous 'destabilizing' force.

4.2. *Neutrally buoyant particles with Cg fixed and a small contact angle*

Next, we investigate the equilibrium configurations for the same contact angle ($\frac{1}{4}\pi$), but with the capillary number increased, holding Cg fixed. As indicated above, this is most easily envisioned as corresponding to a decrease in surface tension, either due to the introduction of surfactants or to a change in the uniform solution temperature, with G and other material parameters held fixed. Figure 8 shows the interface contours for $Cg = 0.01$ and Ca increasing from 0 to 0.0361 and then decreasing back to 0.034 by continuation. The shapes are quite similar to those obtained for an increase in 'flow strength'; however, the interface curvature is slightly less in this case. As seen in figure 9, the decrease in surface tension causes the capillary force to decrease with increasing Ca, even though the contact line position is again moving towards the maximum capillary force configuration. This decrease in the capillary force and the simultaneous increase in the negative viscous force are both balanced in this case by an increase in the buoyancy force.

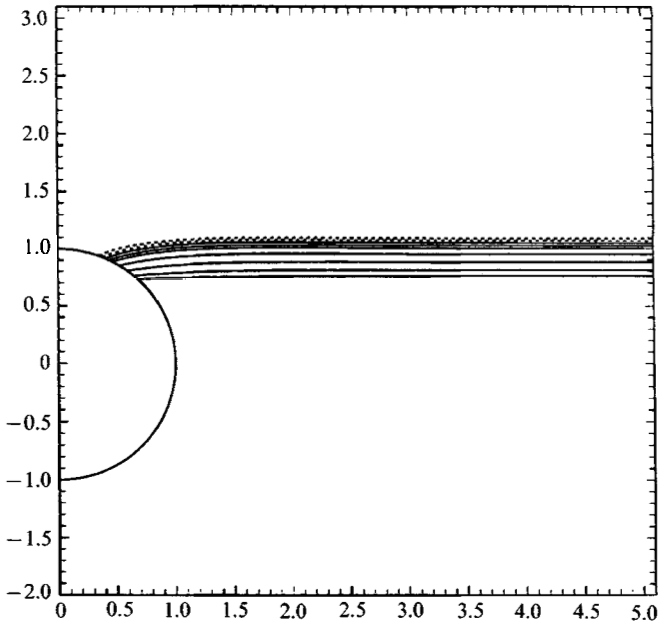

FIGURE 8. Equilibrium sphere/interface configuration for: $\theta_c = \frac{1}{4}\pi$, $\rho_p = \rho$, $Cg = 0.01$: ——, $Ca = 0.01, 0.02, 0.03, 0.035, 0.036, 0.0361$ (stable); - - - - - -, $Ca = 0.0354, 0.0340$ (unstable).

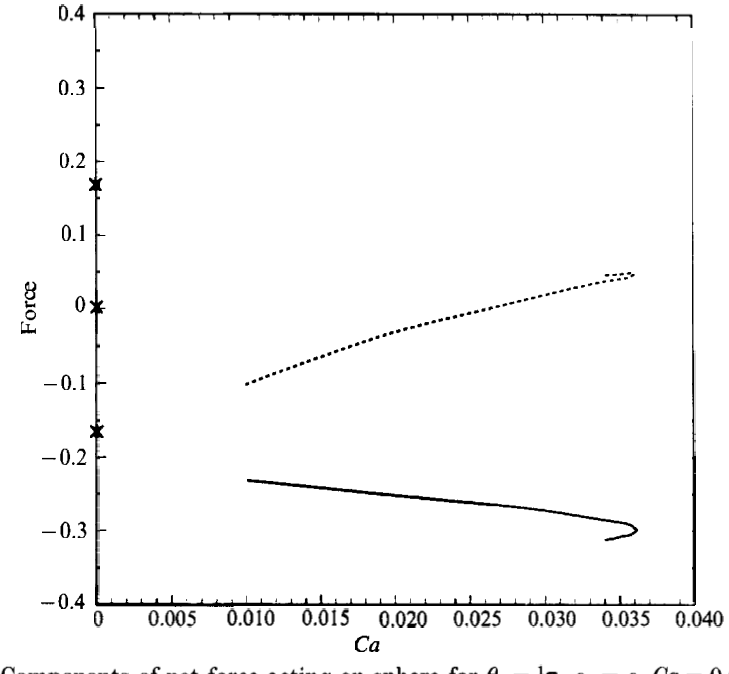

FIGURE 9. Components of net force acting on sphere for $\theta_c = \frac{1}{4}\pi$, $\rho_p = \rho$, $Cg = 0.01$, as a function of capillary number: ——, viscous drag; - - - - - -, net buoyancy force; · · · · · ·, capillary force. Values for $Ca = Cg = 0$ are shown by ×.

It may be noted from figure 9 that the capillary and buoyancy forces, extrapolated toward $Ca = 0$, do not pass through the static values (i.e. $Ca = Cg = 0$). This is because we hold Cg fixed at a constant non-zero value. Thus, from a physical point of view, the limit $Ca \to 0$ with Cg fixed must be interpreted as corresponding to very large surface tension ($\sigma \to \infty$) with 'fixed' flow strength. The solutions shown in figure 8 were obtained with the particle/interface configuration for $Ca = Cg = 0.01$ as an initial condition.

We see, by examining the results in figure 9, that the buoyancy force plays a much more critical role with Cg fixed and Ca increasing, than it did for the case $Ca = Cg$ considered earlier. In particular, in the previous case, the increase of the viscous force with increase of Ca was balanced primarily by a corresponding increase in the capillary force. The changes in the net buoyancy force were also found to resist the tendency for viscous forces to pull the particle from the interface, but always played a secondary role. Here, however, the increase in Ca with Cg fixed can be thought of as resulting from a decrease in surface tension with the strength of the flow held fixed, and the capillary force actually decreases over most of the range of Ca. Hence, it is only the compensating change in the buoyancy force that maintains the sphere on the interface. Indeed, in this case, it is not clear whether the primary reason for the change in interface/sphere configuration with increase of Ca should be thought of as occurring owing to the increased hydrodynamic force, or the decreased capillary force, which changes even faster. In any case, the fact that the net buoyancy force can balance the changes in the capillary and viscous forces is not a consequence of any major change in the dependence of the buoyancy force on Ca, or in the particle–interface configuration relative to the case where $Ca = Cg$. The fact is that the buoyancy force is changed only slightly, and the only reason that it can actually compensate for the increasing viscous force is because the latter is much smaller and varies much more slowly with increase of Ca for Cg fixed than it did for $Ca = Cg$. The reason for this change in the viscous force dependence on Ca is clear upon examination of (14), and is also understood easily in physical terms by again noting that the increase in Ca with Cg fixed can be interpreted as due to a decrease in σ with the flow strength fixed. Hence, in this case, the hydrodynamic force increases with Ca only because the change in configuration with decrease of σ exposes an increasing area of the sphere to the flowing liquid.

In spite of all the differences cited above, relative to the case where $Ca = Cg$, the limit point for increase of Ca with Cg fixed still occurs quite near the configuration (i.e. the value of ϕ) corresponding to the maximum in the capillary force (for a given value of Ca), though the critical capillary number is somewhat larger. In view of the behaviour of the hydrodynamic force discussed above, the small increase in Ca_c from $Ca_c = 0.0327$ to $Ca_c = 0.0361$, as shown in figure 8, is not terribly surprising. What may seem surprising, however, is the apparent connection between the configuration at the limit point, and the maximum capillary force configuration, because it is the increase in the buoyancy force (not capillary force) which compensates for the increase of Ca and maintains stability for almost the entire range of stable values for Ca. Indeed, as we have already noted, the capillary contribution is actually decreasing with increase in Ca and is therefore becoming less, rather than more, of a factor in holding the sphere on the interface. Yet at the final stage, it is the attainment of the angle ϕ where the capillary force is maximum (for a given Ca) that causes the force balance to fail and the limit point to appear. To understand why this occurs, we must examine the results in figure 9 more closely. In particular, if we look at the hydrodynamic force we see that it increases more or less linearly over most of

the range of Ca, but toward the end begins to increase more rapidly. At the same time, the increase in the buoyancy force with Ca begins to slow down. At this stage, to achieve a balance of forces, the system can only respond by trying to increase the capillary force rather than having it continue to decrease. However, this can happen only if the geometric factor in the capillary force (cf. (14)) increases fast enough with the increase in Ca to compensate for the decrease in Ca^{-1}. Hence, small changes in Ca are accompanied by increasingly rapid increases of ϕ, so that in the region very near Ca_c, the capillary force begins to increase and play a critical role in maintaining the force balance on the sphere. Clearly, however, as soon as the maximum capillary force configuration (i.e. the value of $\phi = \phi_{max}$) is reached (for given Ca), the force balance must fail and we hit the limit point that is evident in figures 8 and 9. In fact, the limit point occurs for ϕ slightly smaller than ϕ_{max} as the rate of change of the capillary force with increase in ϕ becomes too weak to sustain the force balance.

A final point concerning the solutions shown in figures 8 and 9 for $\theta_c = \frac{1}{4}\pi$ is the mechanism for instability for the unstable steady configurations that are denoted by the dashed interface contours. The force contributions in figure 9 tell the story, but may appear confusing at first. Specifically, as we pass around the limit point to larger values of ϕ, we see that the hydrodynamic force increases as we would expect, but now the capillary force also increases in spite of the fact that the limit point corresponds to the maximum capillary force configuration for a given value of Ca. The point is that the capillary number on this second solution branch actually decreases with further increase in ϕ, and this compensates for the decrease in the geometric factor in the capillary force. The instability which is characteristic of this branch can only be understood by considering a fluctuation in sphere position, say, for fixed Ca. In this case, any infinitesimal displacement toward increased h will produce an increase in the hydrodynamic force, but without a corresponding increase in the capillary or buoyancy force. Thus, the displacement of the sphere will increase, leading (presumably) to the sphere being pulled from the interface.

4.3. *Neutrally buoyant particle with a large contact angle*

The effects of flow on the existence of equilibrium solutions for a sphere held in an interface is investigated next for a relatively large contact angle, $\theta_c = \frac{8}{9}\pi$. In contrast to the preceding case, $\theta_c = \frac{1}{4}\pi$, where the sphere was strongly 'hydrophillic', and thus only weakly held on the interface by capillary forces, the case $\theta_c = \frac{8}{9}\pi$ corresponds to a strongly hydrophobic particle where the capillary forces are strong and capture should be very stable to the effects of viscous forces in the liquid. Indeed, referring to figure 7, we see that capillary forces are strongly positive for all but very small values of ϕ, and this suggests that it will take much stronger viscous forces to pull the sphere from the interface. This is confirmed in figure 10, where we show equilibrium interface shapes for increasing flow strengths, with $Ca = Cg$ ranging from 0 (static) to the maximum limit point value of 0.304. Comparison with the preceding case where $\theta_c = \frac{1}{4}\pi$ and $Ca_c = 0.0327$ shows that the critical capillary number for capture instability has increased by almost a factor of 10! In other respects, however, the behaviour is qualitatively similar. Specifically, as the flow strength is increased, the increased hydrodynamic force on the sphere is balanced by an increase in the capillary force that is produced by changes in the position of the contact line to larger values of ϕ (and, as we shall see shortly, a decrease in the buoyancy force that is also tending to pull the particle from the interface even in the static state).

The details of the case $Ca = Cg$ with $\theta_c = \frac{8}{9}\pi$ differ, of course, from the cases

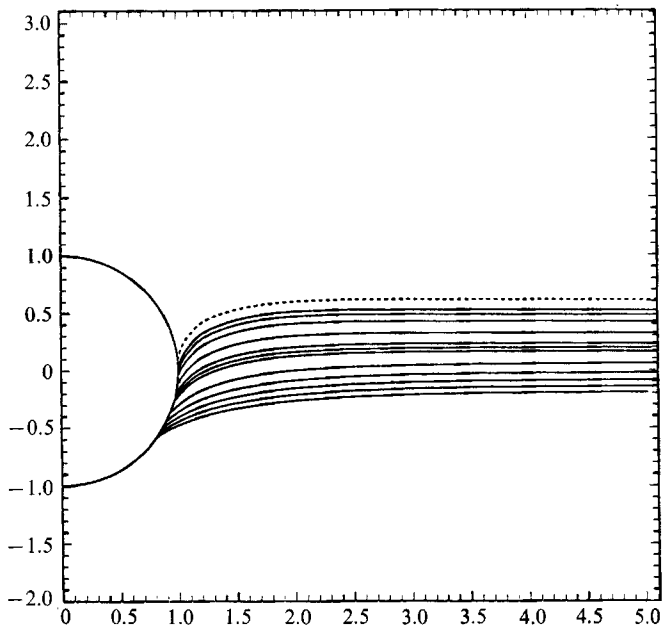

FIGURE 10. Equilibrium sphere/interface configuration for: $\theta_c = \frac{8}{9}\pi$, $\rho_p = \rho$: ——, $Cg = Ca = 0$, 0.05, 0.1, 0.15, 0.2, 0.25, 0.26, 0.27, 0.286, 0.297, 0.302, 0.304 (stable); ------, $Cg = Ca = 0.295$ (unstable).

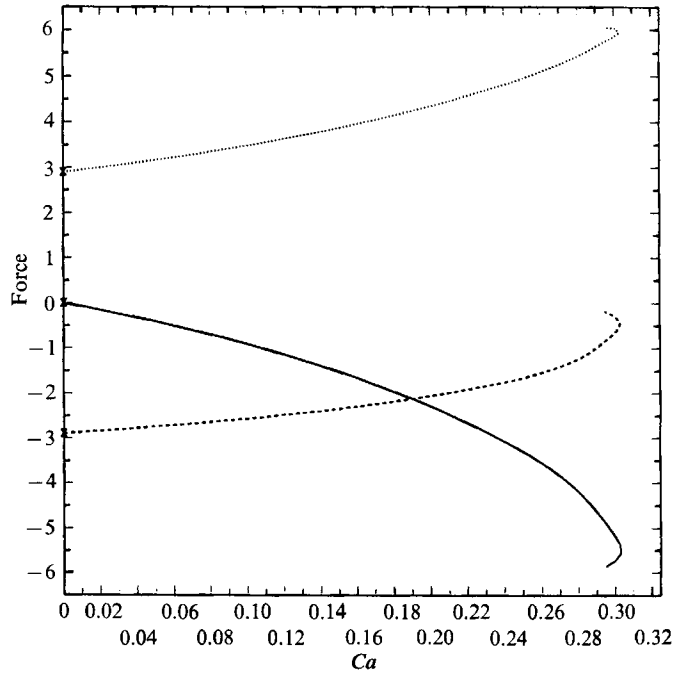

FIGURE 11. Components of net force on sphere for $\theta_c = \frac{8}{9}\pi$, $\rho_p = \rho$, $Cg = Ca$, as a function of capillary number: ——, viscous drag; ------, net buoyancy force; · · · · · ·, capillary force.

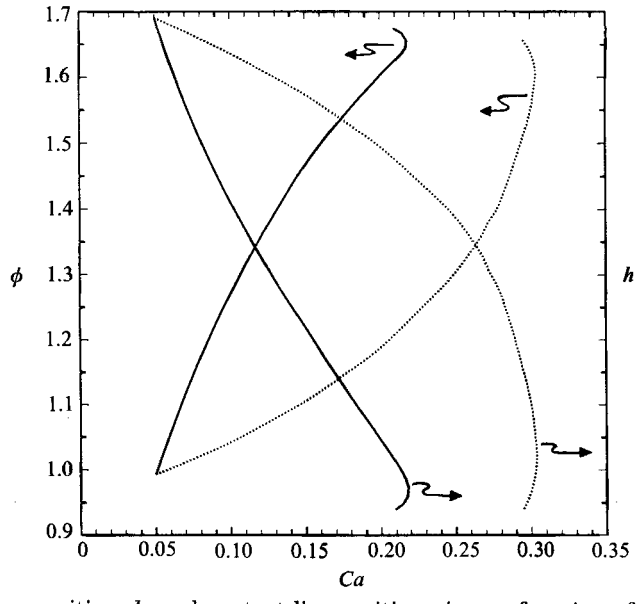

FIGURE 12. Sphere position, h, and contact line position, ϕ, as a function of capillary number for $\theta_c = \frac{8}{9}\pi$, $\rho_p = \rho$: ——, Cg fixed at minimum value of Ca; ·····, $Cg = Ca$.

considered earlier where $\theta_c = \frac{1}{4}\pi$. In particular, the capillary force is now positive and quite large for all but small values of ϕ, and the static equilibrium, representing a balance between capillary forces and buoyancy/body forces, thus occurs for $\phi \sim 30°$. Hence, only a relatively small fraction of the sphere surface is exposed to the lower liquid phase and the hydrodynamic force increases more slowly with increase of Ca than was true in the earlier case. It is this observation, primarily, which accounts for the fact that the critical capillary number increases by almost a factor of 10, while the maximum capillary force attainable increases only by a factor of approximately 6 (see figure 7). In addition, however, since only a small fraction of the sphere is immersed in the liquid, the decreased magnitude of the hydrodynamic force is partially compensated by a much larger net body force which acts in opposition to the capillary force. All of these changes are shown in figures 11 and 12.

In figure 11, we plot the three contributions to the force balance on the sphere as a function of Ca. Figure 12 shows the position of the sphere and contact line, i.e. h and ϕ, also as a function of Ca. It is evident, upon examining figure 11, that the buoyancy and capillary forces are both much larger than for $\theta_c = \frac{1}{4}\pi$. Furthermore, since the initial value of ϕ is much smaller, the increase in ϕ that occurs as a result of the increase in the hydrodynamic force as Ca increases not only produces an increase in the capillary force, but also a decrease in the magnitude of the net buoyancy force. These two changes play an approximately equal role in balancing the hydrodynamic force. The increased importance of the buoyancy contribution is an important change from the small contact angle case that we considered earlier. In spite of this change, however, the limit point still occurs for ϕ which is very close to the maximum capillary force configuration. To understand this, we can examine the behaviour of the three force components in figure 11. In this case, the viscous forces increase faster with increase of Ca until finally the combined effects of buoyancy and capillary forces can no longer compensate. Although this does not occur precisely at the maximum capillary force configuration, the rate of increase of the capillary force

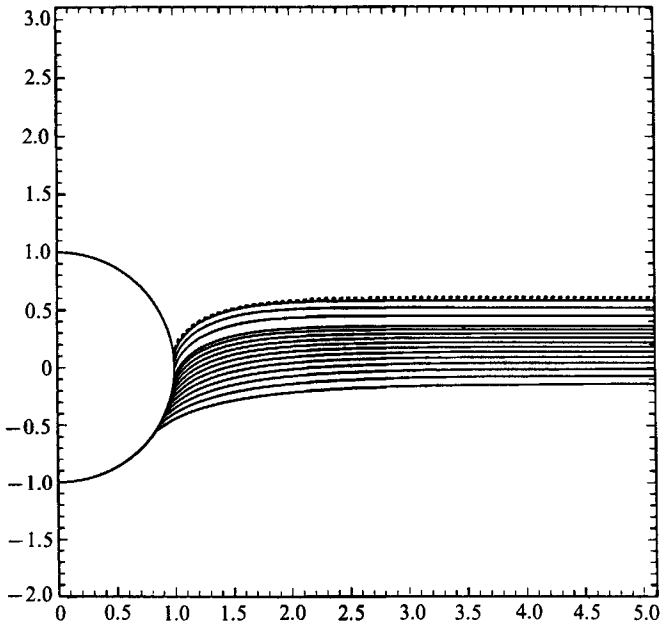

FIGURE 13. Equilibrium sphere/interface configuration for: $\theta_c = \frac{8}{9}\pi$, $\rho_p = \rho$, $Cg = 0.05$: ——, $Ca = 0.05, 0.06, 0.07, 0.08, 0.09, 0.1, 0.11, 0.12, 0.13, 0.14, 0.15, 0.158, 0.184, 0.205, 0.218$ (stable); ------, $Ca = 0.215, 0.206$ (unstable).

with ϕ decreases dramatically as this configuration is approached. A consequence is that the angle ϕ and the sphere position h increase more rapidly as the limit point is approached, as the system attempts to accommodate the increased hydrodynamic force. In the vicinity of the maximum capillary force configuration, however, the combined effect of capillary and buoyancy force increases cannot change fast enough with ϕ and a limit point is reached, beyond which (i.e. for larger Ca) steady solutions do not exist.

For large contact angles, the relative importance of the buoyancy force is even more evident when Ca is increased by decreasing the surface tension while holding the strength of the flow constant (i.e. increasing Ca with Cg fixed). The equilibrium interface shapes for $\theta_c = \frac{8}{9}\pi$, $Cg = 0.05$ and Ca increasing from 0.05 to 0.218 are shown in figure 13. For this case, the limit point (corresponding to capture instability) occurs at a significantly smaller Ca compared to the case $\theta_c = \frac{8}{9}\pi$ with $Ca = Cg$, in spite of the fact that the final contact line and particle positions are approximately the same in the two cases. This behaviour can be explained partly by figure 14, where the various force contributions are shown as a function of Ca. As in figure 9, the capillary force decreases rapidly with increase in Ca, while the hydrodynamic force slowly increases owing to the change in configuration which is caused by the decrease in surface tension. Thus, the buoyancy force must increase to balance both the decrease in the capillary force and the increase in the negative viscous force. As in the case of $\theta_c = \frac{1}{4}\pi$ with Cg fixed, it is probably more accurate, in fact, to think of the changing configuration with increase in Ca as being due to the decreasing capillary force rather than an increase in hydrodynamic force as in the cases where $Ca = Cg$. The existence of a limit point, as shown in figure 14, is harder to explain in this case. It would appear from the results in figure 14 to be due to the decreasing rate of increase in the buoyancy force with Ca, which means that it

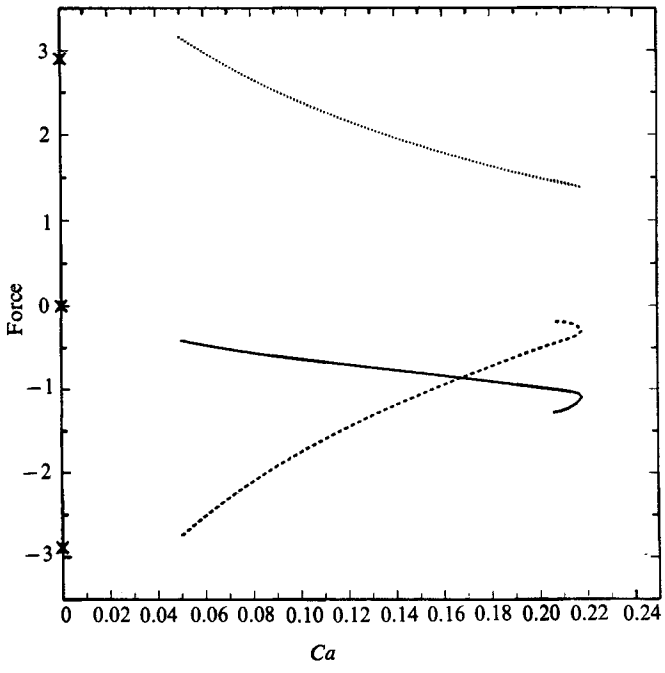

FIGURE 14. Components of net force acting on sphere for $\theta_c = \frac{8}{9}\pi$, $\rho_p = \rho$, $Cg = 0.05$, as a function of capillary number: ——, viscous drag; ------, net buoyancy force; · · · · · ·, capillary force. Values for $Ca = Cg = 0$ are shown by ×.

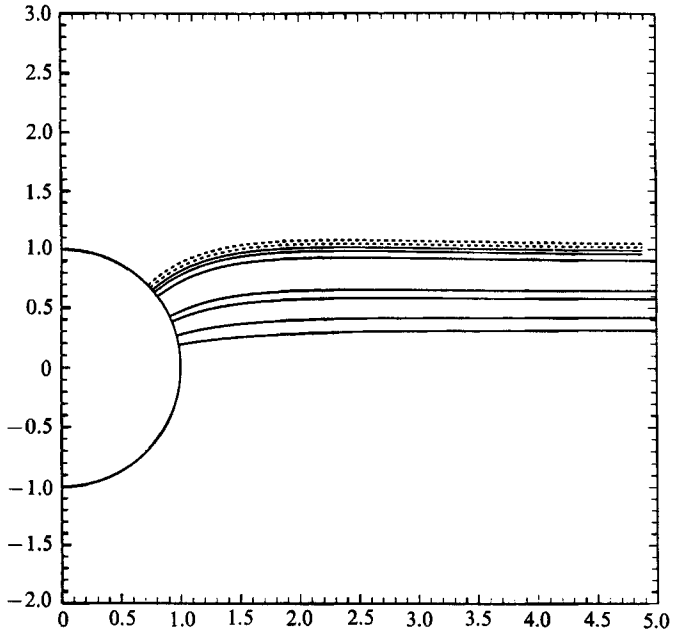

FIGURE 15. Equilibrium sphere/interface configuration for: $\theta_c = \frac{1}{2}\pi$, $\rho_p = \rho$: ——, $Cg = Ca = 0$, 0.05, 0.1, 0.11, 0.125, 0.1255, 0.1256 (stable); ------, $Cg = Ca = 0.1251$, 0.1246 (unstable).

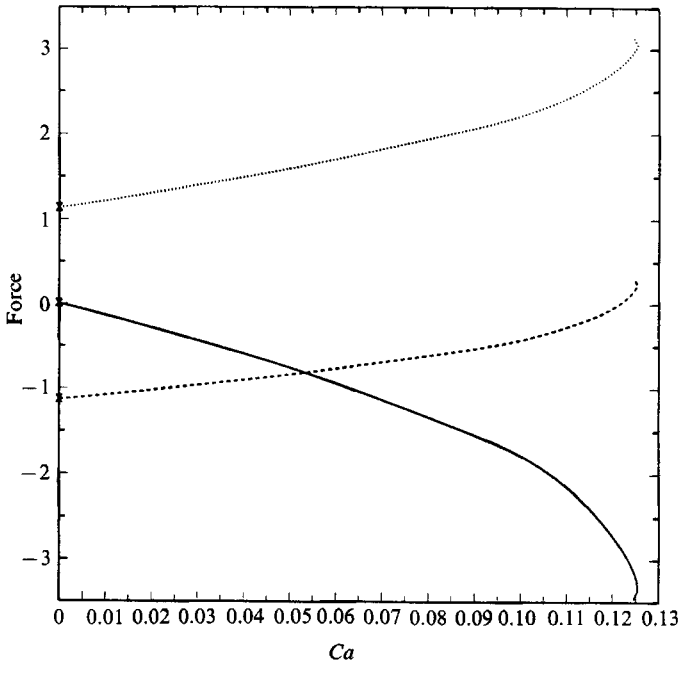

FIGURE 16. Components of net force acting on sphere for $\theta_c = \frac{1}{2}\pi$, $\rho_p = \rho$, $Cg = Ca$, as a function of capillary number: ——, viscous drag; ------, net buoyancy force; · · · · · ·, capillary force.

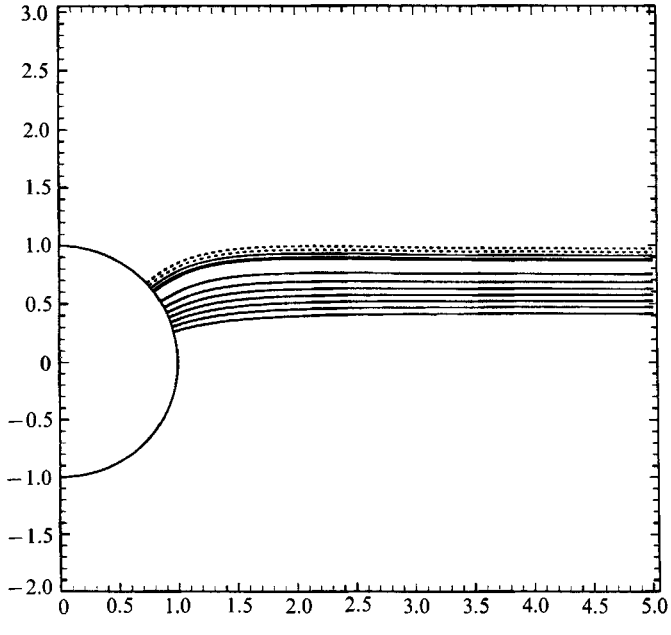

FIGURE 17. Equilibrium sphere/interface configuration for: $\theta_c = \frac{1}{2}\pi$, $\rho_p = \rho$, $Cg = 0.05$: ——, $Ca = 0.05$, 0.06, 0.07, 0.08, 0.09, 0.1, 0.11, 0.12, 0.1205, 0.1211 (stable); ------, $Ca = 0.1210$, 0.1202 (unstable).

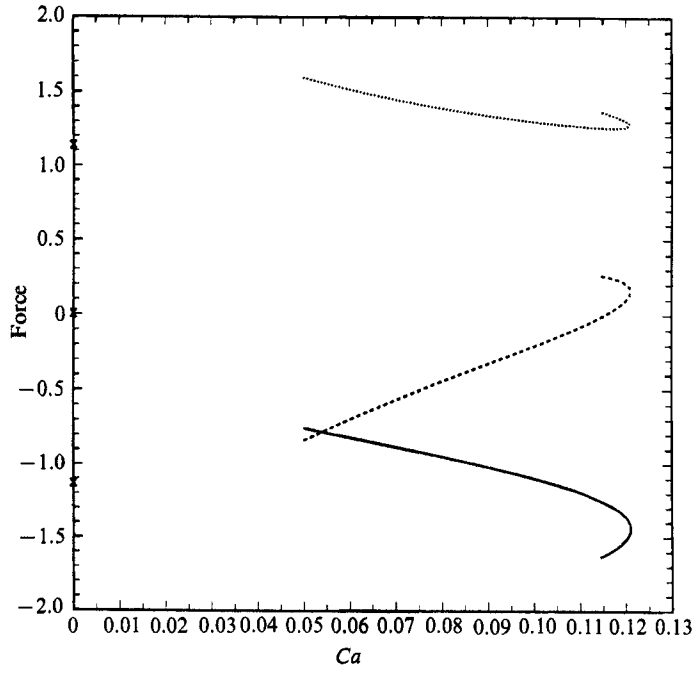

FIGURE 18. Components of net force acting on sphere for $\theta_c = \frac{1}{2}\pi$, $\rho_p = \rho$, $Cg = 0.05$, as a function of capillary number: ——, viscous drag; ------, net buoyancy force; · · · · · ·, capillary force.

eventually cannot compensate for the constant increasing hydrodynamic force and the rapidly decreasing capillary force. This may, in fact, be the proper explanation. However, it is noteworthy from figures 6 and 7 that the configuration at the limit point does not correspond to an extremum in the buoyancy force, but does lie close to the maximum capillary force configuration. In view of the fact that the changes in the capillary force with Ca are 'destabilizing' rather than stabilizing and the lack of anything 'special' about the capillary force dependence on Ca near Ca_c, this is difficult to understand.

4.4. *Neutrally buoyant particles with intermediate contact angles*

The final situation investigated in detail is the case where the contact angle is intermediate between strongly wetting and non-wetting, $\theta_c = \frac{1}{2}\pi$. The interface contours and magnitude of the forces acting on the particle for the situation where Ca is increased by increasing the flow strength ($Cg = Ca$) are shown in figures 15 and 16, respectively. Also, the interface contours and magnitude of the forces acting on the particle for the situation where Ca is increased by decreasing the surface tension ($Cg = 0.05$) are shown in figures 17 and 18. The sphere position and contact angle position are shown in figure 19. For both of these cases, it is clear that the equilibrium interface shape and final equilibrium configuration are very similar for the two cases. Furthermore, the behaviour is very much an image of the two cases $\theta_c = \frac{1}{4}\pi$ and $\theta_c = \frac{8}{9}\pi$, and we shall therefore not discuss it again here.

Before concluding this section, however, we wish to briefly discuss two special cases; first a case involving very small values of the contact angle (a fluid which strongly wets the particle surface so that the particle is difficult to capture in a flotation process), and, second, a case involving a non-neutrally buoyancy particle.

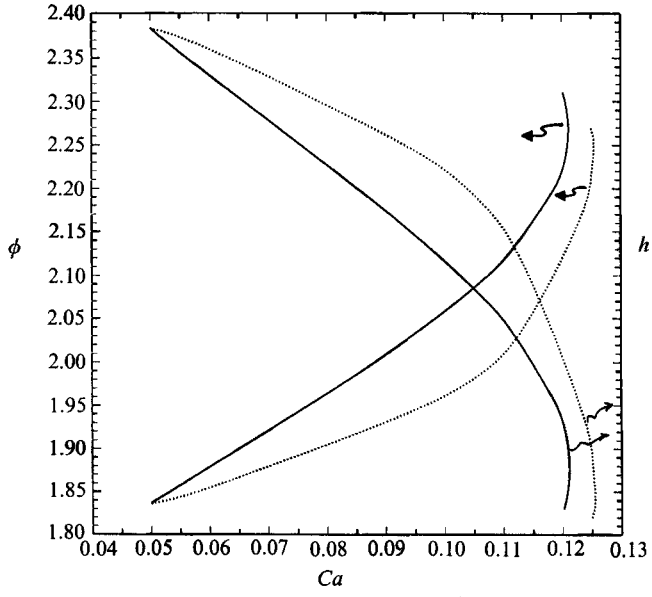

FIGURE 19. Sphere position, h, and contact line position, ϕ, as a function of capillary number for $\theta_c = \frac{1}{2}\pi$, $\rho_p = \rho$: ——, Cg fixed at minimum value of Ca; ·····, $Cg = Ca$.

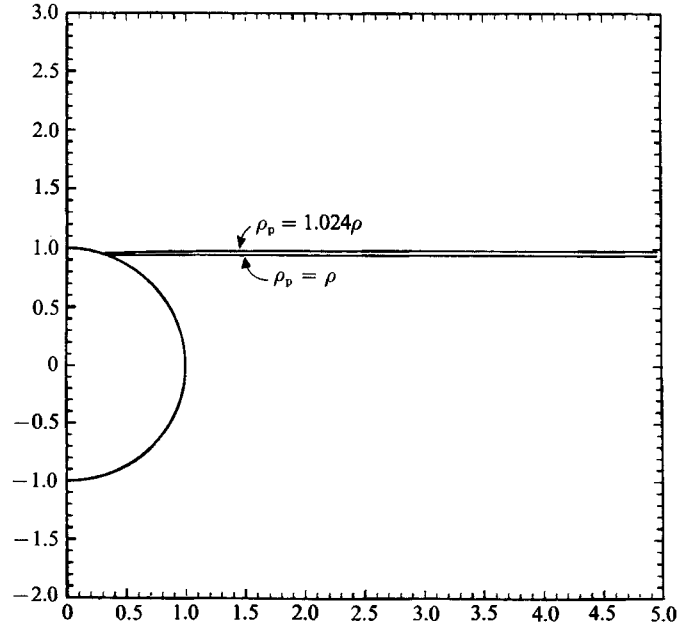

FIGURE 20. Equilibrium sphere/interface configuration for: $\theta_c = \frac{1}{9}\pi$; $\rho_p = \rho$, and $\rho_p = 1.024\rho$ (critical particle density).

4.5. *Subcritical contact angles for capture stability*

It was noted earlier that an attempt was made to obtain steady-state solutions, in the presence of flow, for a contact angle, $\theta_c = \frac{1}{9}\pi$. However, we were unable to obtain steady-state solutions, even for extremely weak flows with $Ca = Cg = 0.01$. It had

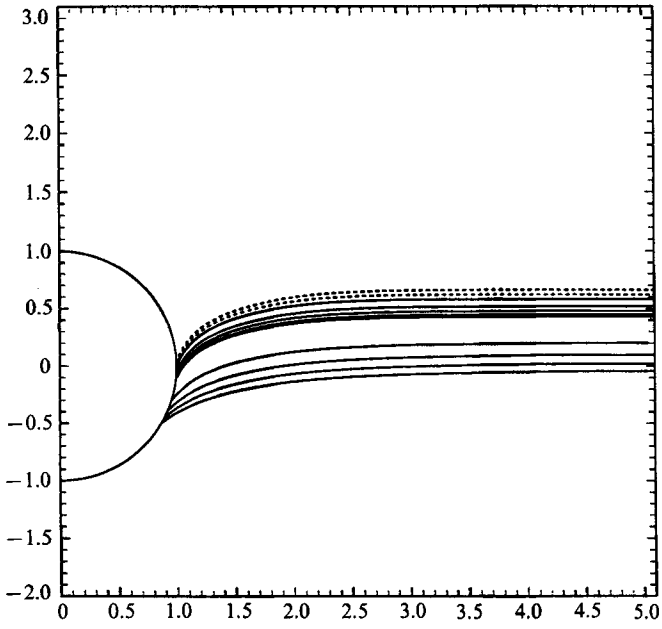

FIGURE 21. Equilibrium sphere/interface configuration for: $\theta_c = \frac{8}{9}\pi$, $\rho_p = 1.25\rho$: ——, $Cg = Ca = 0$, 0.05, 0.1, 0.15, 0.2, 0.2005, 0.2015, 0.2022, 0.2028 (stable); ------, $Cg = Ca = 0.2014$, 0.1991 (unstable).

been noted earlier, by Boucher & Jones (1981), that only extremely small particles with density very close to that of the fluid, i.e. $\rho_p/\rho \approx 1$, can achieve a stable equilibrium configuration for small θ_c, even in the static limit. The interface contours for $Ca = Cg = 0$ are plotted in figure 20 for $\rho_p/\rho = 1$, and for $\rho_p/\rho = 1.024$. These interface contours are plotted relative to a coordinate system fixed at the centre of the particle. For $\rho_p/\rho > 1.024$, no steady-state solutions could be attained. With the knowledge gained from the case $\theta_c = \frac{1}{4}\pi$, discussed earlier, we can now understand this sensitivity to ρ_p/ρ and the resultant difficulty of affecting separations by flotation for systems with a small contact angle. The difficulty for small θ_c is that there is only a very small range of contact line positions, with $\phi \approx \pi$, where the capillary force acts in the positive z-direction and thus has potential to support a particle against the net 'buoyancy' force (or, in the presence of flow, the viscous force) which acts to pull the particle from the interface. Even in this range of ϕ, the maximum magnitude of the capillary force is very small. This can be seen most clearly by examining the variation in the capillary force as a function of contact line position for $\theta_c = \frac{1}{9}\pi$, as shown in figure 7. The capillary force is positive only for $2.8 < \phi < 3.14$, and the maximum magnitude is smaller than 0.2. In this case, only infinitesimal flows can be withstood by a neutrally buoyant particle with $Ca = Cg < 0.01$.

4.6. *The effect of particle density*

An indication of the effect of particle density on the equilibrium configuration is shown in figure 21, where equilibrium sphere–interface configurations are shown for a particle of density $\rho_p = 1.25\rho$ with $\theta_c = \frac{8}{9}\pi$ and increasing values of $Ca = Cg$. These configurations may be compared with figure 10, where the neutral-density particle is considered for the same θ_c. This comparison is purposely made for large contact angles, since we expect the changes in the particle surface area that is exposed to the

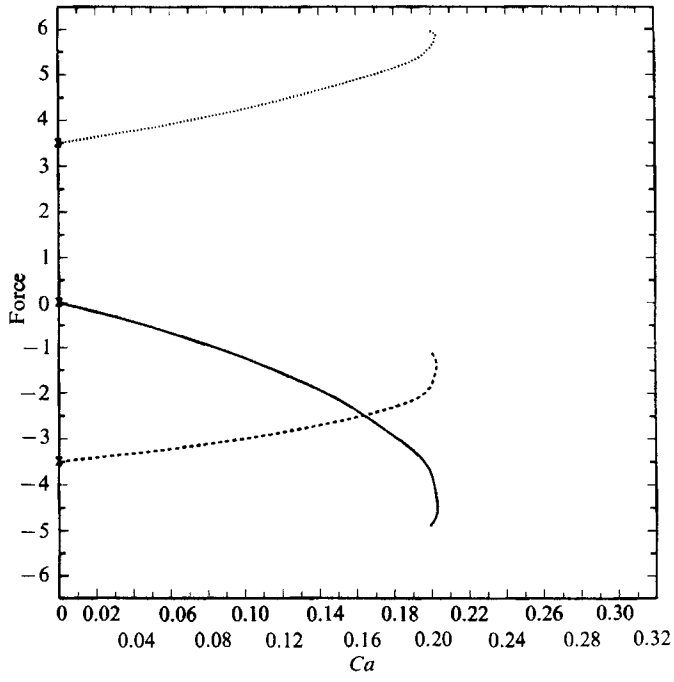

FIGURE 22. Components of net force acting on sphere for $\theta_c = \frac{8}{9}\pi$, $\rho_p = 1.25\rho$, $Cg = Ca$, as a function of capillary number: ——, viscous drag; ------, net buoyancy force; ·····, capillary force.

flow, due to increases in the flow strength, to be largest for this case, thus presumably increasing the sensitivity of the results to changes in the particle density. In comparing figures 10 and 21, we note that the critical capillary number falls from 0.3 to 0.2 with the increase in particle density. Also, the interface is significantly less curved near the particle for the large particle density case, no doubt as a result of the lower critical flow rate. The difference in the interface shapes in figures 10 and 21 is one indication of the complicated interactions between the flow field, the interface shape, and the force balance on the particle. The decrease in critical capillary number occurs partly owing to the additive contribution of the extra body force. Comparing the neutral buoyant particle forces in figure 11 with the dense particle forces in figure 22, the critical capillary force is nearly the same; however, the buoyant force is more negative for the dense particle and thus only a smaller viscous drag and critical capillary number can be withstood. However, the interaction is nonlinear, as can be seen from figure 23, where the sphere position as a function of capillary number is plotted from figures 10 and 21. Although the shapes of the curves are similar, if one were to attempt to extrapolate between the results for the neutral-density flow case and the dense static particle case to obtain the critical capillary number for a dense particle in a flow, the estimated value of Ca would be off by at least 0.05, as can be seen from the shifted form of the curve for $\rho_p = 1.25\rho$. Thus, we conclude that estimates of the combined effects of flow and particle density, obtained by a simple interpolation between the flow effects described in this paper and the effects of particle density described in Boucher & Jones (1981) will be in error because of the nonlinear interactions of these effects. However, it is not difficult to obtain solutions for various particle densities and flow strengths using the method outlined in this paper.

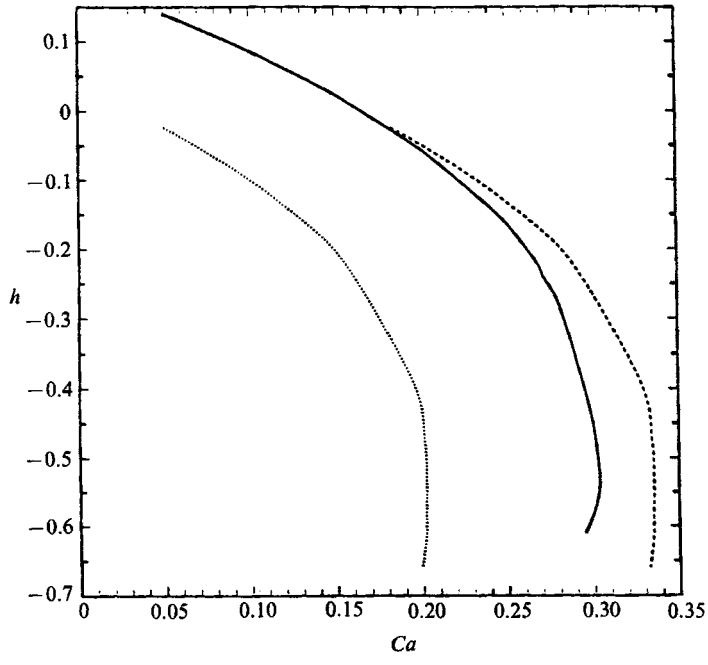

FIGURE 23. Sphere position, h, as a function of capillary number for $\theta_c = \frac{8}{9}\pi$, $Cg = Ca$: ——, $\rho_p = \rho$; · · · · · ·, $\rho_p = 1.25\rho$; ------, $\rho_p = 1.25\rho$ (shifted to compare with $\rho_p = \rho$).

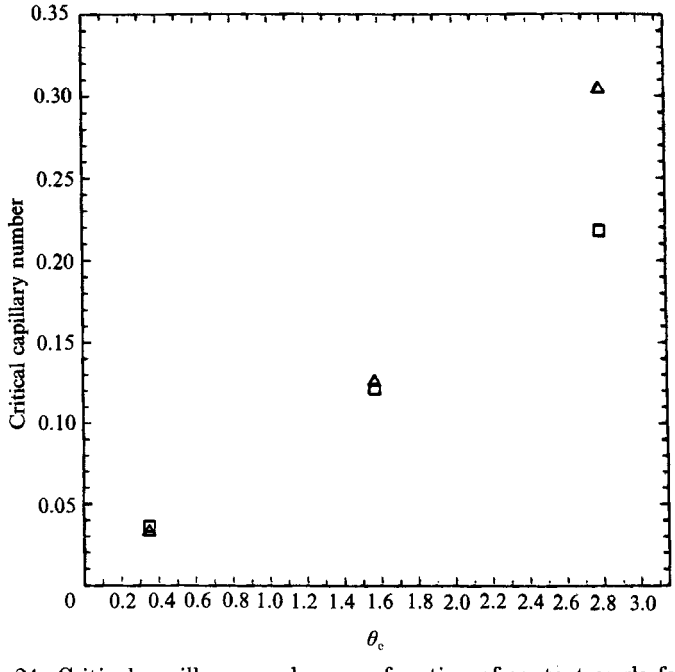

FIGURE 24. Critical capillary number as a function of contact angle for: △, $Cg = Ca$; □, Cg = constant (minimum value of Ca).

4.7. *Critical conditions for capture stability*

Finally, as a guide in calculating the range of selective separations that may be possible through use of the flow field, the critical capillary numbers for all cases considered in this paper with neutral density particles are shown in figure 24. The critical capillary number falls rapidly for small contact angles because of the decreased effectiveness of the restoring capillary force. Also, there can be a significant difference in the critical capillary number between the cases where changes in Ca result from increased flow, and cases where changes in Ca result from decreased surface tension. This difference again points up the increased relative importance of buoyancy forces at large capillary number. From these critical capillary numbers, the maximum particle size that can be separated or the minimum contact angle for a particle of fixed size could be calculated for a given system with all other parameters specified.

5. Conclusions

Even a very small amount of flow can greatly affect the stability of particles that are 'captured' at a fluid interface, especially for small contact angles. Even for large contact angles, corresponding to hydrophobic particles, the flow has a significant effect on the particle–interface configuration and the stability of captured particles, but the effects are seen at larger capillary numbers. The effects of increasing the capillary number by increasing the flow strength (i.e. with $Ca = Cg$) or decreasing the surface tension (i.e. Cg fixed) are smaller for large contact angles because the capillary restoring force is larger for large contact angles and also because the viscous destabilizing force is smaller, since less of the particle is exposed to the lower fluid.

The configuration at which the critical capillary number is reached is surprisingly invariant to changes in the contact angle. For small contact angles, the contact line position, ϕ, at which the final equilibrium solution is found, coincides closely with the contact line position at which the capillary force reaches a maximum for the given contact angle. Since the net buoyancy force is small for small contact angles, the viscous force balances the capillary force. Beyond the critical (or limit) point, increases in the flow strength or decreases in the surface tension cannot be balanced by increases in the capillary force since this force is already at a maximum, and a steady-state configuration is not possible. For large contact angles, the contact line position at the critical capillary number is still close to the contact line position where the capillary force reaches a maximum. This is more difficult to understand because in this case changes in the buoyancy force compensate for increases in Ca over most of the range of Ca values.

Appendix A. Contact point determination

A two-point right-handed difference scheme is used to determine the contact line position such that the contact angle has the desired value. In the representation for the interface, $z = f(r)$, the contact line radial position (which is undetermined) is denoted as r_0, the first node point on the interface is r_1, the second node point on the interface is r_2, and so on. The vertical positions of the interface at the first and second

node points can be represented in terms of Taylor series expansions about the contact line position as

$$f(r_0+\Delta r_1) = f(r_0)+\Delta r_1 f'(r_1)+\tfrac{1}{2}\Delta r_1^2 f''(r_0)+\ldots, \tag{A 1}$$

$$f(r_0+\Delta r_1+\Delta r_2) = f(r_0)+(\Delta_1+\Delta r_2)f'(r_1)+\tfrac{1}{2}(\Delta r_1+\Delta r_2)^2 f''(r_0)+\ldots, \tag{A 2}$$

where, $\Delta r_1 = r_1-r_0$, $\Delta r_2 = r_2-r_1$. Combining these two equations, we obtain

$$f(r_0) = \left[\left(\frac{\Delta r_1+\Delta r_2}{\Delta r_1}\right)^2 f(r_1)-f(r_2)-(\Delta r_1+\Delta r_2)f'(r_0)\frac{\Delta r_2}{\Delta r_1}\right] \times\left[\left(\frac{\Delta r_1+\Delta r_2}{\Delta r_1}\right)^2-1\right]^{-1}. \tag{A 3}$$

The slope of the interface at the contact line, $f'(r_0)$, is determined by the macroscopic contact angle and the geometry of the problem as

$$f'(r_0) = \tan(\phi+\theta_c) = \frac{\tan\phi+\tan\theta_c}{1-\tan\theta_c\tan\phi}, \tag{A 4}$$

where, $\tan\phi = r_0/(1-r_0^2)^{\frac{1}{2}}$. And the condition that the first node point lies on the sphere is

$$f(r_0) = h+(1-r_0^2)^{\frac{1}{2}}. \tag{A 5}$$

Substituting (A 4) and (A 5) into (A 3), we obtain a nonlinear algebraic equation for r_0, in terms of the known values h, r_1, r_2, $f(r_1)$, $f(r_2)$ and θ_c. The old value of r_0 is used as an initial guess along with a Newton's method scheme to solve this relation for r_0, the new contact line position on the sphere which satisfies the required macroscopic contact angle.

Appendix B. Static shape determination

In this Appendix, we describe our method for calculating the particle–interface configuration for the static (no-flow) case. Although the statics problem has been considered by a number of previous workers, our method involves some modifications which enable a straightforward calculation of the particle–interface configuration given the physical parameters of the system, rather than being forced to set one of these parameters (e.g. particle size) to satisfy the force balance on the particle.

The Young–Laplace equation represents the balance between the hydrostatic pressure difference across the interface because of different densities in the upper and lower fluids and the surface tension force because of the interface curvature. In terms of figure 1, it can be expressed in the form

$$\sigma\left(\frac{\dfrac{\mathrm{d}^2z}{\mathrm{d}r^2}}{\left[1+\left(\dfrac{\mathrm{d}z}{\mathrm{d}r}\right)^2\right]^{\frac{3}{2}}}+\frac{\dfrac{\mathrm{d}z}{\mathrm{d}r}}{r\left[1+\left(\dfrac{\mathrm{d}z}{\mathrm{d}r}\right)^2\right]^{\frac{1}{2}}}\right)-g\rho z = 0. \tag{B 1}$$

Equation (B 1) is a second-order nonlinear ordinary differential equation for the interface shape, expressed as $z = f(z)$, which must be solved subject to the boundary conditions

$$\frac{\mathrm{d}z}{\mathrm{d}r} = \tan\beta_0 \quad \text{at} \quad r = r_0, \tag{B 2}$$

$$\left.\begin{matrix} \dfrac{\mathrm{d}z}{\mathrm{d}r} \to 0 \\ z \to 0 \end{matrix}\right\} \quad as \quad r \to \infty. \tag{B 3}$$

In addition to the basic nonlinearity of the problem, the solution of (B 1) is complicated by the fact that boundary conditions (B 2) and (B 3) comprise a two-point boundary-value problem with one of the boundaries at infinity. This must be solved numerically and the interface truncated at some large but finite value of r. The method used in the present work for the solution of the statics problem is similar in many respects to that used by Rapacchietta & Neumann (1977), and Huh & Scriven (1969).

In the static problem it is convenient to non-dimensionalize lengths by $l_c = (\sigma/g\rho)^{\frac{1}{2}}$, so that $y \equiv z/l_c$ and $x \equiv r/l_c$. After parameterizing the interface in terms of the angle of inclination, β (shown in figure 1), one obtains (Huh & Scriven 1969)

$$\frac{\mathrm{d}x}{\mathrm{d}\beta} = \frac{x\cos\beta}{xy - \sin\beta}, \tag{B 4}$$

$$\frac{\mathrm{d}y}{\mathrm{d}\beta} = \frac{x\sin\beta}{xy - \sin\beta} \tag{B 5}$$

with boundary conditions

$$x = x_0, \quad y = y_0 \quad \text{at} \quad \beta = \beta_0, \tag{B 6}$$

$$y \to 0, \quad x \to \infty \quad \text{as} \quad \beta \to 0. \tag{B 7}$$

The net force on the particle at equilibrium is given by

$$F_{\text{net}} = \left(-\tfrac{4}{3}\pi\frac{\rho_{\text{p}}}{\rho} - \pi\frac{h}{a}\sin^2\phi - \tfrac{2}{3}\pi\cos^3\phi + \tfrac{2}{3}\pi\right) - 2\pi\sin\phi\sin(\phi+\theta_c)\left\{\frac{\sigma}{a^2 g\rho}\right\} = 0, \tag{B 8}$$

where the last term is the ratio $Cg/Ca = (l_c/a)^2$, the ratio of surface tension forces to density forces, which is equivalent to the ratio of the two lengthscales in the problem. The relations arising from the geometry of the problem are

$$\phi = \beta_0 + \pi - \theta_c, \tag{B 9}$$

$$x_0 = \frac{a}{l_c}\sin(\beta_0 - \theta_c), \tag{B 10}$$

$$y_0 = -\frac{h}{l_c} + \frac{a}{l_c}\cos(\beta_0 - \theta_c), \tag{B 11}$$

where x_0, y_0, and β_0 are the values of x, y, and β at the contact line. With $a\hat{a}$, θ_c and ρ_p/ρ specified, the physical problem is determined and the mathematical problem is well posed with h, β_0 and the shape all determined as part of the solution.

This solution is obtained by the shooting method since interpolation via the tables of Huh & Scriven, combined with iteration on the force balance, is inaccurate and slow. The method of Rapacchietta & Neumann is modified to calculate the full sphere position and interface shape that satisfies the force balance on the sphere, rather than calculating the net force with an assumed contact line position, and iterating on the particle size until the force balance is satisfied. A difficulty arises because the starting point x_0, y_0 and shooting angle β_0 are all unknown. The method of solution involves: guessing β_0; calculating ϕ from (B 9); with this value of ϕ the force balance is solved for $(h/l_c)h$, and then x_0 and y_0 are determined from (B 10) and (B 11); finally, (B 4) and (B 5) are integrated using a fourth-order predictor–corrector method from β_0 to some sufficiently small value of $\beta\,(=\beta_f)$ close to zero where boundary condition (B 7) is checked for $y \approx 0$. If this condition is not satisfied, a new β_0 is chosen. The new β_0 is calculated using Newton's method such that the new values of β_0, x_0 and y_0 produce a y_f that is closer to zero. Since x and y are coupled, the effect of x_0, y_0 and β_0 on both x and y must be computed. Thus,

$$\frac{\mathrm{d}x}{\mathrm{d}\beta} = f(x, y, \beta), \tag{B 12}$$

$$\frac{\mathrm{d}y}{\mathrm{d}\beta} = g(x, y, \beta). \tag{B 13}$$

We define

$$\epsilon \equiv \frac{\partial x}{\partial y_0}, \quad \gamma \equiv \frac{\partial x}{\partial \beta_0}, \quad \xi \equiv \frac{\partial x}{\partial x_0}, \tag{B 14}$$

$$\eta \equiv \frac{\partial y}{\partial y_0}, \quad \delta \equiv \frac{\partial y}{\partial \beta_0}, \quad \alpha \equiv \frac{\partial y}{\partial x_0}. \tag{B 15}$$

The dependence of x and y on x_0, y_0 and β_0 is given by

$$\frac{\partial}{\partial x_0}\left(\frac{\mathrm{d}x}{\mathrm{d}\beta}\right) = \frac{\mathrm{d}}{\mathrm{d}\beta}\left(\frac{\partial x}{\partial x_0}\right) = \frac{\mathrm{d}\xi}{\mathrm{d}\beta} = \frac{\partial f}{\partial x}\frac{\partial x}{\partial x_0} + \frac{\partial f}{\partial y}\frac{\partial y}{\partial x_0} = f_x\xi + f_y\alpha, \tag{B 16}$$

$$\frac{\partial}{\partial x_0}\left(\frac{\mathrm{d}y}{\mathrm{d}\beta}\right) = \frac{\mathrm{d}}{\mathrm{d}\beta}\left(\frac{\partial y}{\partial x_0}\right) = \frac{\mathrm{d}\alpha}{\mathrm{d}\beta} = \frac{\partial g}{\partial x}\frac{\partial x}{\partial x_0} + \frac{\partial g}{\partial y}\frac{\partial y}{\partial x_0} = g_x\xi + g_y\alpha, \tag{B 17}$$

$$\frac{\partial}{\partial y_0}\left(\frac{\mathrm{d}x}{\mathrm{d}\beta}\right) = \frac{\mathrm{d}}{\mathrm{d}\beta}\left(\frac{\partial x}{\partial y_0}\right) = \frac{\mathrm{d}\epsilon}{\mathrm{d}\beta} = \frac{\partial f}{\partial x}\frac{\partial x}{\partial y_0} + \frac{\partial f}{\partial y}\frac{\partial y}{\partial y_0} = f_x\epsilon + f_y\eta, \tag{B 18}$$

$$\frac{\partial}{\partial y_0}\left(\frac{\mathrm{d}y}{\mathrm{d}\beta}\right) = \frac{\mathrm{d}}{\mathrm{d}\beta}\left(\frac{\partial y}{\partial y_0}\right) = \frac{\mathrm{d}\eta}{\mathrm{d}\beta} = \frac{\partial g}{\partial x}\frac{\partial x}{\partial y_0} + \frac{\partial g}{\partial y}\frac{\partial y}{\partial y_0} = g_x\epsilon + g_y\eta, \tag{B 19}$$

$$\frac{\partial}{\partial \beta_0}\left(\frac{\mathrm{d}x}{\mathrm{d}\beta}\right) = \frac{\mathrm{d}}{\mathrm{d}\beta}\left(\frac{\partial x}{\partial \beta_0}\right) = \frac{\mathrm{d}\gamma}{\mathrm{d}\beta} = \frac{\partial f}{\partial x}\frac{\partial x}{\partial \beta_0} + \frac{\partial f}{\partial y}\frac{\partial y}{\partial \beta_0} = f_x\gamma + f_y\delta, \tag{B 20}$$

$$\frac{\partial}{\partial \beta_0}\left(\frac{\mathrm{d}y}{\mathrm{d}\beta}\right) = \frac{\mathrm{d}}{\mathrm{d}\beta}\left(\frac{\partial y}{\partial \beta_0}\right) = \frac{\mathrm{d}\delta}{\mathrm{d}\beta} = \frac{\partial g}{\partial x}\frac{\partial x}{\partial \beta_0} + \frac{\partial g}{\partial y}\frac{\partial y}{\partial \beta_0} = g_x\gamma + g_y\delta. \tag{B 21}$$

The coefficients f_x, f_y, g_x and g_y are Rapacchietta & Neumann as

$$f_x(x, y, \beta) = \frac{(-\sin\beta\cos\beta)}{(xy-\sin\beta)^2}, \tag{B 22}$$

$$f_y(x, y, \beta) = \frac{(-x^2\cos\beta)}{(xy-\sin\beta)^2}, \tag{B 23}$$

$$g_x(x, y, \beta) = \frac{(-\sin^2\beta)}{(xy-\sin\beta)^2}, \tag{B 24}$$

$$g_y(x, y, \beta) = \frac{(-x^2\sin\beta)}{(xy-\sin\beta)^2}. \tag{B 25}$$

Now the procedure is to integrate (B 4), (B 5) and (B 16)–(B 21) simultaneously from the initial conditions β_0 with

$$\epsilon_0 = 0, \quad \eta_0 = 1, \quad \xi_0 = 1, \quad \alpha_0 = 0, \quad \gamma_0 = -\frac{a}{l_c}\cos(\beta_0-\theta_c)$$

$$\delta_0 = \frac{8\,a/l_c\,\rho_p\cos(\beta_0-\theta_c)}{3\rho\sin^3(\beta_0-\theta_c)} - \frac{2\cos\beta_0}{a/l_c\sin(\beta_0-\theta_c)} + \frac{2\sin\beta_0\cos(\beta_0-\theta_c)}{a/l_c\sin^2(\beta_0-\theta_c)}$$
$$- \frac{2\,a/l_c\cos^2(\beta_0-\theta_c)}{\sin(\beta_0-\theta_c)} - \frac{4\,a/l_c\cos^4(\beta_0-\theta_c)}{3\sin^3(\beta_0-\theta_c)} - \frac{4\,a/l_c\cos(\beta_0-\theta_c)}{3\sin^3(\beta_0-\theta_c)}$$

to the point β_f. Then y_f is compared to zero and x_f is checked to see whether it is sufficiently large. If these conditions are not met Newton's method is used to increment β_0 to β_0'

$$\beta_0' = \beta_0 - w\frac{y(\beta_f)}{\left.\dfrac{dy}{d\beta_0}\right|_{\beta_f}},$$

$$\left.\frac{dy}{d\beta_0}\right|_{\beta_f} = \left.\frac{\partial y}{\partial\beta_0} + \frac{\partial y}{\partial x_0}\frac{\partial x_0}{\partial\beta_0} + \frac{\partial y}{\partial y_0}\frac{\partial y_0}{\partial\beta_0}\right|_{\beta_f},$$

where w is a relaxation factor $\leqslant 1$, used to prevent divergence of the solution. The entire procedure is then repeated until $y_f \approx 0$ and $x_f > R_0$ the truncation distance.

REFERENCES

Boucher, E. A. & Evans, M. J. B. 1975 Pendant drop profiles and related capillary phenomena. *Proc. R. Soc. Lond.* A **346**, 349

Boucher, E. A., Evans, M. J. B. & Kent, H. J. 1976 Capillary phenomena. II. Equilibrium and stability of rotationally symmetric fluid bodies. *Proc. R. Soc. Lond.* A **349**, 81.

Boucher, E. A. & Jones, T. G. J. 1981 Empirical criteria for the flotation of a solid sphere at an interface in a gravitational field. *J. Colloid Interface Sci.* **83**, 645.

Boucher, E. A. & Kent, H. J. 1977 Capillary phenomena III. Properties of rotationally symmetric fluid bodies with one asymptote – holms. *Proc. R. Soc. Lond.* A **356**, 61.

Boucher, E. A. & Kent, H. J. 1978 Capillary phenomena Part 6. – Behavior associated with the flotation and mechanical manipulation of solid spheres at fluid interfaces. *J. Chem. Soc. Faraday Trans.* I **74**, 846.

CHI, B. & LEAL, L. G. 1987 A theoretical study of the motion of a viscous drop toward a fluid interface at low Reynolds number. *J. Colloid Interface Sci.* (Accepted.)

DAVIS, A. M. J. 1982 Two phase Stokes flows distorted by a sphere straddling the interface. *Intl J. Multiphase Flow* **8**, 361.

DERJAGUIN, B. V. & DUKHIN, S. S. 1981 Kinetic theory of the flotation of fine particles. In *Proc. 13th Intl Mineral Processing Congr., Warsaw, 1979*. Elsevier.

DUSSAN V., E. B. 1979 On the spreading of liquids on solid surfaces: static and dynamic contact lines. *Ann. Rev. Fluid Mech.* **11**, 371.

FALADE, A. 1982 Arbitrary motion of an elliptic disc at a fluid interface. *Intl J. Multiphase Flow* **8**, 543.

FRENCH, R. M. & WILSON, D. J. 1980 Fluid mechanics – foam flotation interactions. *Sep. Sci. Tech.* **15**, 1213.

GELLER, A. S., LEE, S. H. & LEAL, L. G. 1986 The creeping motion of a spherical particle normal to a deformable interface. *J. Fluid Mech.* **169**, 27.

GIRAULT, H. H. J., SCHIFFRIN, D. J. & SMITH, B. D. V. 1982 Drop image processing for surface and interfacial tension measurements. *J. Colloid Interface Sci.* **137**, 207.

GIRAULT, H. H. J., SCHIFFRIN, D. J. & SMITH, B. D. V. 1984 The measurement of interfacial tension of pendent drops using a video image digitizer. *J. Electroanal. Chem.* **101**, 257.

HIEMENZ, P. C. 1977 *Principles of Colloid and Surface Chemistry*, Ch. 6. New York: Dekker.

HUH, C. & MASON, S. G. 1974 The flotation of axisymmetric particles at horizontal liquid interfaces. *J. Colloid Interface Sci.* **47**, 271.

HUH, C. & SCRIVEN, L. E. 1969 Shapes of axisymmetric fluid interfaces of unbounded extent. *J. Colloid Interface Sci.* **30**, 323.

IOOSS, G. & JOSEPH, D. D. 1980 *Elementary Stability and Bifurcation Theory*. Springer.

IVANOV, I. B., KRALCHEVSKY, P. A. & NIKOLOV, A. D. 1985 Film and line tension effects on the attachment of particles to an interface I. Conditions for mechanical equilibrium of fluid and solid particles at a fluid interface. *J. Colloid Interface Sci.* **112**, 97.

KANTOROVICH, L. V. & KRYLOV, V. I. 1958 *Approximate Methods of Higher Analysis*. Interscience.

KRALCHEVSKY, P. A., IVANOV, I. B. & NIKOLOV, A. D. 1985 Film and line tension effects on the attachment of particles to an interface II. Shapes of the bubble (drop) and the external meniscus. *J. Colloid Interface Sci.* **112**, 108.

KRALCHEVSKY, P. A., NIKOLOV, A. D. & IVANOV, I. B. 1985 Film and line tension effects on the attachment of particles to an interface IV. Experimental studies with bubbles in solutions of dodecyl sodium sulfate. *J. Colloid Interface Sci.* **112**, 132.

KUBICEK, M. & MAREK, M. 1983 *Computational Methods in Bifurcation Theory and Dissipative Structures*. Springer.

LADYZHENSKAYA, O. A. 1969 *The Mathematical Theory of Viscous Incompressible Flow*. Gordon and Breach.

LEE, S. H. & LEAL, L. G. 1982 Motion of a sphere in the presence of a deformable interface. Part 2: numerical study of the translation of a sphere normal to an interface. *J. Colloid Interface Sci.* **87**, 81.

NIKOLOV, A. D., KRALCHEVSKY, P. A. & IVANOV, I. B. 1985 Film and line tension effects on the attachment of particles to an interface III. A differential interferometric method for determination of the shapes of fluid surfaces. *J. Colloid Interface Sci.* **112**, 122.

PRINCEN, H. M. 1963 Shape of a fluid drop at a liquid–liquid interface. *J. Colloid Interface Sci.* **18**, 178.

PRINCEN, H. M. & MASON, S. G. 1965*a* Shape of a fluid drop at a fluid–liquid interface I. Extension and test of a two phase theory. *J. Colloid Interface Sci.* **20**, 156.

PRINCEN, H. M. & MASON, S. G. 1965*b* Shape of a fluid drop at a fluid–liquid interface II. Theory for three-phase systems. *J. Colloid Interface Sci.* **20**, 246.

RALLISON, J. M. & ACRIVOS, A. 1978 A numerical study of the deformation and burst of a viscous drop in an extensional flow. *J. Fluid Mech.* **89**, 191.

RANGER, K. B. 1978 The circular disk straddling the interface of two-phase flow. *Intl J. Multiphase Flow* **4**, 263

RAPACCHIETTA, A. V. & NEUMANN, A. W. 1977 Force and free-energy analysis of small particles at fluid interfaces II. Spheres. *J. Colloid Interface Sci.* **59**, 555.

RAPACCHIETTA, A. V., NEUMANN, A. W. & OMENYI, S. N. 1977 Force and free-energy analysis of small particles at fluid interfaces I. Cylinders. *J. Colloid Interface Sci.* **59**, 541.

ROTENBERG, Y., BORUVKA, L. & NEUMANN, A. W. 1983 Determination of surface tension and contact angle from the shapes of axisymmetric fluid interfaces. *J. Colloid Interface Sci.* **93**, 169.

ROTENBERG, Y., BORUVKA, L. & NEUMANN, A. W. 1984 The shape of nonaxisymmetric drops on inclined planar surfaces. *J. Colloid Interface Sci.* **102**, 424.

SADHAL, S. S. & JOHNSON, R. E. 1983*a* Stokes flow past bubbles and drops partially coated with thin films. Part 1. Stagnant cap of surfactant film-exact solutions. *J. Fluid Mech.* **126**, 237.

SADHAL, S. S. & JOHNSON, R. E. 1983*b* Stokes flow past bubbles and drops partially coated with thin films. Part 2. Thin films with internal circulation – a perturbation solution. *J. Fluid Mech.* **132**, 295.

SMITH, P. G. & VEN, T. G. M. VAN DE 1984 The effect of gravity on the drainage of a thin liquid film between a solid sphere interface and a liquid/fluid interface. *J. Colloid Interface Sci.* **100**, 456.

STONE, H. A., BENTLEY, B. J. & LEAL, L. G. 1986 An experimental study of transient effects in the breakup of viscous drops. *J. Fluid Mech.* **173**, 131.

STOOS, J. A. 1987 Ph.D. dissertation. California Institute of Technology.

SUTHERLAND, K. L. & WARK, I. W. 1955 *Principles of Flotation.* Melbourne: Australian Institute of Mining and Metallurgy.

YOUNGREN, G. K. & ACRIVOS, A. A. 1975 Stokes flow past a particle of arbitrary shape: a numerical method of solution. *J. Fluid Mech.* **69**, 377.

YOUNGREN, G. K. & ACRIVOS, A. A. 1976 On the shape of a gas bubble in a viscous extensional flow. *J. Fluid Mech.* **76**, 433.